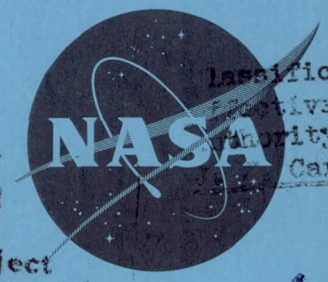

TECHNICAL MEMORANDUM
X-338

SOME AERODYNAMIC AND CONTROL STUDIES OF

LIFTING REENTRY CONFIGURATIONS AT ANGLES OF ATTACK

UP TO 90° AT A MACH NUMBER OF 2.91

By Frank L. Clark and Joanna M. Evans

Langley Research Center
Langley Field, Va.

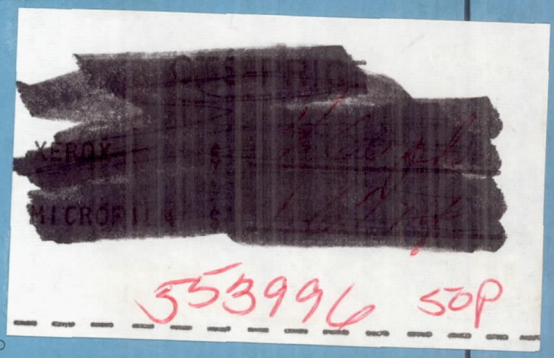

NATIONAL AERONAUTICS AND SPACE ADMINISTRATION

WASHINGTON November 1960

NATIONAL AERONAUTICS AND SPACE ADMINISTRATION

TECHNICAL MEMORANDUM X-338

SOME AERODYNAMIC AND CONTROL STUDIES OF LIFTING REENTRY CONFIGURATIONS AT ANGLES OF ATTACK UP TO 90° AT A MACH NUMBER OF 2.91*

By Frank L. Clark and Joanna M. Evans

SUMMARY

An investigation has been conducted in the Langley 9-inch supersonic tunnel at a Mach number of 2.91 to determine the stability and control characteristics of four triangular-wing lifting reentry configurations. The configurations were chosen as being typical of an airplane-like configuration which might reenter the earth's atmosphere at maximum lift or at an angle of attack of 90°. Longitudinal control for all models was provided by flaps which extended beyond the trailing edge of each wing. Rectangular holes were provided on each wing just ahead of the leading edge of the flaps in an effort to increase flap effectiveness. Directional stability was provided by 6.5° toed-in fins located at the tip of each wing. One model was tested over an angle-of-attack range from -4° to 90° for flap conditions ranging from the no-flap case to flap deflections of ±90°. This model was also tested over an angle-of-sideslip range of 4° to -15° at angles of attack up to 81°. Tests on the other three models were restricted to angles of attack below 36° and flap deflections of 0° and 5°.

Results indicated that, for all flap deflections, maximum lift occurred at an angle of attack of 48°; however, the model could not be trimmed near this point. Values of maximum lift coefficient varied from about 0.73 to 0.80, depending on the flap deflection. Decreasing the flap deflection from 0° to -50° (rectangular holes opened) increased the trim angle of attack from 2° to about 12° and, for angles of attack greater than 15°, made the model neutrally stable over a large portion of the test angle-of-attack range. The presence of the rectangular holes had very little effect in increasing flap effectiveness. For flap deflections in the range from 50° to -50°, flap effectiveness increased as angle of attack was increased up to about 70°; further increase in angle of attack generally resulted in a reduction in flap effectiveness.

The model was directionally stable at angles of attack of 0° and 30°.

*Title, Unclassified.

INTRODUCTION

A reentry vehicle which uses lift during reentry into the earth's atmosphere offers a number of advantages over a vehicle which uses a ballistic reentry. One scheme for performing the reentry maneuver requires a vehicle which can fly near its maximum lift coefficient over a large portion of the reentry trajectory. Theoretical calculations show that the ability of the vehicle to attain a high lift coefficient can have a significant effect on the reduction of the heat load for which the vehicle must be designed and that the heat input encountered during reentry can be reduced on a vehicle by using a large leading-edge radius and highly swept wings. An alternate reentry-maneuver scheme specifies that the vehicle reenter the earth's atmosphere at 90° angle of attack and that when the vehicle has slowed to a Mach number of about 2, it is nosed over into a conventional flight attitude. The design of the model used in the present investigation was primarily intended for the former type of reentry maneuver (near maximum lift); however, so little information exists on winged configurations at an angle of attack near 90° that the tests on one of the configurations were conducted through a complete angle-of-attack range to 90°.

Although heating and minimum weight will, to a large extent, govern the design of a reentry vehicle, there are a number of stability and control problems connected with a reentry maneuver which need solutions. The primary purpose of the present investigation is to contribute experimental information which will aid in the design of a winged reentry vehicle which can be trimmed at angles of attack near maximum lift and will be longitudinally and directionally stable. The models employed in the investigation do not provide a configuration which can fly in a trimmed condition near maximum lift for the center-of-gravity location selected, but by using the information furnished to design stabilizing and control surfaces and by employing other means, such as nose cant, a flyable configuration could be developed.

The present investigation presents the results of some aerodynamic and control studies on four basic triangular wing configurations suitable for lifting reentry. Tests were conducted at a free-stream Mach number of 2.91, angles of attack up to 90°, combined angles of attack and sideslip, and flap deflections as large as $\pm 90^\circ$.

SYMBOLS

b wing span, in.

$\bar{c}$ mean aerodynamic chord (based on distance from theoretical apex to wing trailing edge), in.

C_D drag coefficient, $\frac{\text{Drag}}{q_\infty S}$

C_L lift coefficient, $\frac{\text{Lift}}{q_\infty S}$

C_m pitching-moment coefficient, $\frac{\text{Pitching moment}}{q_\infty S\bar{c}}$

C_N normal-force coefficient, $\frac{\text{Normal force}}{q_\infty S}$

C_n yawing-moment coefficient (wind-axis system), $\frac{\text{Yawing moment}}{q_\infty Sb}$

C_Y side-force coefficient (wind-axis system), $\frac{\text{Side force}}{q_\infty S}$

L/D lift-drag ratio

l length of sting, measured from schlieren-window center line (positive upstream from vertical axis of schlieren-window center line), in.

M Mach number

q dynamic pressure, lb/sq in.

S total wing area (including theoretical apex, see table I), sq in.

$x_{ac}/\bar{c}$ aerodynamic-center location, $\partial C_m/\partial C_N$

α angle of attack, deg

β angle of sideslip, deg

δ flap-deflection angle, positive deflection downward, deg

Subscripts:

δ flap-deflection angle, deg

∞ free stream

APPARATUS AND TESTS

Wind Tunnel and Balance

The investigation was conducted in the Langley 9-inch supersonic tunnel of the High Temperature Fluid Mechanics Section. This tunnel is a continuous, closed-return type of tunnel with provisions for the control of the humidity, temperature, and pressure of the enclosed air. During the tests the quantity of water vapor in the tunnel air was kept sufficiently low so that the effect of water condensation in the supersonic nozzle was negligible.

Force data were measured with an external mechanical balance. Balance design details may be found in the appendix of reference 1.

Models and Model Design Considerations

Drawings illustrating design features, pertinent dimensions, and model designations are presented in figure 1. Geometric properties of the models, such as wing area and aspect ratio, are presented in table I.

The wing trailing edge of model A was recessed to accommodate any one of eleven sets of interchangeable flaps. Each set of flaps was constructed to produce different flap deflections. The wing and flaps of the other three models (B, C, and D) were constructed as one unit and had a flap deflection of 0°; the only exception was model B which could also be tested with a flap deflection of 5°. Model A and model B utilized the same body with the wing of model B one-half as thick as the wing of model A. Model C was a flat-bottom configuration and model D was a midwing configuration. All models had hemicylindrically rounded wing and flap leading edges.

The flaps of each model extended beyond the trailing edge of the wing. This type of configuration could be considered as representative of drawer-type flaps on a full-scale vehicle with the flaps extended. The flaps might be used for both longitudinal and roll control; however, only longitudinal control is considered in this investigation. The rectangular holes cut through the wings just ahead of the flaps would normally act as a receptacle for the flaps; also the presence of the holes could possibly increase flap effectiveness by permitting the air to bleed through the holes onto the leeward side of the flaps for positive angles of attack and negative flap deflections.

The tip fins were toed-in 6.5° on all models. The majority of tests conducted on model A were with the tip fins canted outward approximately 15° in an attempt to increase their directional effectiveness at high

angles of attack; tests on the other three models were conducted with the tip fins not canted.

Tests

All tests were conducted at a free-stream Mach number of 2.91. Longitudinal tests were conducted on model A over an angle-of-attack range from -4° to 90° for configurations with no flaps and for configurations with flap deflections of 0°, $\pm 20^\circ$, and $\pm 50^\circ$. In general, testing of the other flap deflections, as well as testing of the other three models, was restricted to angles of attack below 36°. In order to determine if the presence of the rectangular holes increased flap effectiveness, tests were conducted on model A with the holes covered up. The closed-hole tests covered the complete angle-of-attack range for configurations with no flaps and configurations with flap deflections of 0° and $\pm 20^\circ$. All tests were conducted at a Reynolds number per inch of about 0.204×10^6.

In order to test model A over the complete angle-of-attack range it was necessary to employ two different stings and two different model-mounting techniques. All models were sting supported from the base of the model body for angles of attack as high as 36°. A straight sting and a 30° bent sting were used to obtain angles of attack from -4° to 15° and 15° to 36°, respectively. In order to obtain angles of attack greater than 36° it was necessary to mount the stings in a hole located at the top of the body just ahead of the model base. (See fig. 1(a).) By affixing the stings in this location, testing was permitted in the angle-of-attack range from 36° to 63° with the bent sting inverted and from 66° to 90° with the straight sting. It should be mentioned that some sting and support interference was experienced when the model was tested at large angles of attack. A more detailed discussion of the interference is presented in appendix B.

Directional tests were conducted on model A for a 0° flap deflection over an angle-of-sideslip range from -4° to 15° at angles of attack of 0°, 30°, 50°, and 81°. A limited number of tests were conducted on model A with the tip fins not canted to determine if canting improved the tip-fin effectiveness.

A movable windshield shielded the stings from the external flow. The shield extended to within 0.030 inch of the model. At angles of attack up to 36° the model base pressure was measured by means of four orifices located in the windshield. The average base pressure was used to estimate the base drag, and all force data were corrected to the condition of free-stream base pressure. At angles of attack greater than 36° (stings mounted in top of model body), this correction was applied only to the area occupied by the windshield.

Angles of attack and sideslip were determined optically by using a 1/16-inch-diameter mirror, flush mounted in the model, to reflect and focus a spot from a high-intensity light source onto a previously calibrated scale. By using this method the true angle could be obtained irrespective of the model deflection under load.

Accuracy

The estimated accuracies of the final data as affected by uncertainties in the measurements of the forces, free-stream static pressure, and free-stream dynamic pressures are presented below.

C_L	±0.001
C_D	±0.0002
C_m	±0.002
C_Y	±0.001
C_n	±0.002

Angles of attack and sideslip are estimated to be accurate to within $\pm 0.1^\circ$.

RESULTS AND DISCUSSION

Schlieren Photographs

Typical schlieren photographs of model A (rectangular holes opened, $\delta = 0^\circ$) are presented in figure 2 for various angles of attack. The photographs show that a strong normal shock emanates from the rounded leading edge of the flap, an indication that high heat-transfer rates would be encountered in this region on a flight vehicle.

Basic Aerodynamic Characteristics

Results of the tests are presented in figures 3 to 14 with aerodynamic coefficients plotted against angle of attack, angle of sideslip, and flap-deflection angle. Figures 3 and 4 show some scatter in the data, particularly in the pitching-moment coefficient. It was suspected and subsequently confirmed that this scatter was due to sting and balance support interference. Appendices A and B present results of some auxiliary tests which were conducted to explore the possibility of extraneous effects on the data. Appendix A shows that

there are no effects on the data due to the possibility of flow condensation on the leeward side of the wing at high angles of attack. Appendix B shows the results of tests which were conducted to illustrate any sting interference effects at 90° angle of attack. For the 90° angle-of-attack case some sting interference was present on the drag results.

Longitudinal Aerodynamic and Control Characteristics

The longitudinal aerodynamic characteristics of model A (rectangular holes opened) are presented in figure 3. These data show that maximum lift occurs at an angle of attack of about 48° for the flap deflections tested. Maximum lift-coefficient values of from about 0.73 to 0.80 are shown, depending on the flap deflection. In general, for all positive flap deflections, the model was stable up to the maximum lift coefficient. At higher angles of attack, the model developed a pitchup tendency which became progressively more pronounced as flap deflection was increased. With the exception of $\delta = -90°$, decreasing flap deflection increased the relative magnitude of the pitching-moment coefficient and made the model neutrally stable over a large portion of the angle-of-attack range.

The model trimmed at an angle of attack near 0° for flap deflections of 0° and 90°; however, no trim points existed for any other positive flap deflections. In the lower range of angle of attack ($\alpha = 0°$ to 15°) decreasing flap deflection increased the trim angle of attack from 2° to about 12°; at high angles of attack, the data showed that for flap deflections of -20° and -50° the model had both stable and unstable trim points throughout the angle-of-attack range.

The longitudinal aerodynamic characteristics of model A (rectangular holes covered) are presented in figure 4. In general, covering the rectangular holes reduced the magnitude of the pitching-moment coefficient and increased the value of the maximum lift coefficient. Maximum lift coefficient still occurred at an angle of attack of approximately 48°.

The basic data for model B are presented in figure 5 for flap deflections of 0° and 5°. A data comparison between model A and model B is presented in figure 6. Decreasing the wing thickness by a factor of one-half caused the model to become neutrally stable for flap deflections of 0° and 5°. As would be expected there was a decrease in drag coefficient and a corresponding increase in maximum L/D.

The basic data for model C and model D are presented in figures 7 and 8. Results indicate that both models are longitudinally stable over the test angle-of-attack range. The flat-bottom configuration (model C) had a slightly higher L/D and a slightly greater lift-curve slope.

The effects of angle of attack on the aerodynamic-center location for model A (rectangular holes open) are presented in figure 9 for various flap deflections. It should be mentioned that fairing the pitching-moment curves for the various flap deflections (fig. 3) was somewhat arbitrary because of the considerable amount of scatter in the data. Therefore, the results presented in figure 8 should only be used to indicate trends. In general, the aerodynamic center for all flap deflections moved forward slowly with increasing angle of attack for $0 < \alpha < 45^\circ$. When angles of attack up to about 45° are considered, the configurations with negative flap deflections showed a sudden decrease in stability near $\alpha \approx 20^\circ$ which did not occur for the configurations with positive flap deflections. At an angle of attack of about 45° the aerodynamic center for positive flap deflections moved forward very rapidly. A maximum value of aerodynamic-center position occurred at about $\alpha = 56^\circ$. The aerodynamic center for negative and 0° flap deflections had approximately the same maximum forward location. In all cases the aerodynamic center moved rapidly rearward with increase in angle of attack once the maximum forward location had been obtained.

Flap Effectiveness

Incremental values of lift and pitching-moment coefficients of model A are plotted against flap-deflection angle in figure 10 for specific angles of attack. The data presented in the plots were obtained by taking the test value of the coefficient for a specific angle of attack and flap deflection and subtracting from it the test value of the coefficient at the same angle of attack for a flap deflection of 0°.

Figure 10 shows that there is a negative incremental lift coefficient produced by small positive flap deflection (0° to 20°) at angles of attack of 60° and above. The pitching-moment data do not show a corresponding reversal, although the data for small flap deflections ($\pm 20^\circ$) and high angles of attack (80° and 90°) show that the flaps are not effective under these circumstances. The fact that a reversal in lift coefficient does not cause a corresponding reversal in pitching-moment coefficient is attributed to the fact that increasing flap deflection also produces a drag force on the flaps which acts below the model moment reference and creates a negative pitching moment.

A decreasing incremental lift coefficient with increasing positive flap deflection might be expected when the sum of the flap-deflection angle and the angle of attack are greater than the angle for maximum lift. The data presented in figure 10 do not closely follow this expected trend. For example, the lift-coefficient results at $\alpha = 50^\circ$ show an increasing lift coefficient as the flap-deflection angle increases from 0° to 20°. This case corresponds to increasing the angle of the flaps with respect to the free-stream direction from 50° to 70°.

Referring to the incremental pitching-moment data of figure 10 shows that, for flap deflections in the range from 50° to -50°, no loss in flap effectiveness occurred as the angle of attack was increased up to about 70°; further increase in angle of attack produced a reduction in flap effectiveness. Flap deflections of ±90° were completely ineffective at angles of attack up to 50°; however, a reversal in flap effectiveness was experienced at an angle of attack of 90° and the flaps did become slightly effective. If a vehicle corresponding to model A could fly at an angle of attack of 90°, a nose-forward moment would be obtained with a positive flap deflection of 90° and a nose-rearward moment would be obtained with a negative flap deflection of 90°.

Effect of Rectangular Holes

The effect of the rectangular holes ahead of the leading edge of the drawer-type flap is shown in figure 11 wherein incremental lift and pitching-moment coefficients are plotted against flap-deflection angle for specific angles of attack. The presence of the rectangular holes had very little effect on the values of the coefficients when the incremental values were referenced to a flap deflection of 0°. However, significant differences in the values were noted when the incremental values were referenced to the no-flap condition.

Sideslip Characteristics

The sideslip characteristics of model A (rectangular holes opened and 0° flap deflection) are presented in figure 12. The variation of side force with β reverses direction at an angle of attack slightly less than 30°. For the low-angle-of-attack case a negative sideslip angle produces a positive side force as might be expected. The negative side force which occurs for negative sideslip angles at high angles of attack results simply from the fact that there is a component of the normal force of the wing which contributes to the side force.

Yawing-moment results for angles of attack greater than 30° are not presented because of inability to repeat the data during check runs. These discrepancies are believed to have been caused by some small amount of roll which was unintentionally set in the model when it was alined in the tunnel. The yawing-moment results of figure 12 show that the model is directionally stable at angles of attack of 0° and 30°.

At 0° angle of attack the drag coefficient increases with sideslip angle and at 81° angle of attack the drag coefficient decreases with sideslip angle.

The effect of canting the small tip fins on model A is shown in figure 13 for angles of attack of 0° and 30°. Figure 14 shows the effect of canting the large tip fin for an angle of attack of 50°. The results indicate that canting these tip fins outward approximately 15° produced only slight effects on the sideslip characteristics.

CONCLUSIONS

An investigation made at a Mach number of 2.91 to determine the aerodynamic and control characteristics of four lifting reentry configurations indicated the following conclusions:

1. For configurations with rectangular holes ahead of the flaps, maximum lift-coefficient values of from about 0.73 to 0.80 were obtained, depending on the flap deflection. Slightly higher values were obtained with no holes ahead of the flaps. The maximum lift coefficient occurred at an angle of attack of about 48° for all test configurations.

2. A midwing configuration had a slightly lower lift-curve slope and a slightly lower lift-drag ratio than a similar flat-bottom configuration. Another configuration comparison showed that, by decreasing the wing thickness by one-half, lift-drag ratios could be increased. Decreasing wing thickness decreased the longitudinal stability of the model as might be expected.

3. The presence of rectangular holes ahead of the leading edge of each flap had very little effect on the incremental values of lift and pitching-moment coefficients for flap deflections of ±20°.

4. For flap deflections between 50° and -50° no loss in flap effectiveness occurred as the angle of attack was increased up to about 70°; further increase in angle of attack resulted in a reduction in flap effectiveness. Flap deflections of 90° or -90° were completely ineffective at angles of attack up to 50°; however, the flaps did become slightly effective at an angle of attack of 90°.

5. The configuration which was tested in sideslip was directionally stable at angles of attack of 0° and 30°. Canting the tip fins outward approximately 15° had no significant effect on the directional stability at the test angles of attack.

Langley Research Center,
National Aeronautics and Space Administration,
Langley Field, Va., July 7, 1960.

APPENDIX A

DEWPOINT CONSIDERATIONS

The moisture content of the wind tunnel was kept sufficiently low (dewpoint, -10° F and below) to prevent any flow condensation in the test section; however, because of the large amount of expansion required of the free stream when the models were tested at high angles of attack, it was speculated that some flow condensation could conceivably be realized on the leeward side of the model. If some condensation did result, it might have some effect on the measured force data and could possibly explain the scatter in the data. In an effort to determine this effect, a limited number of tests were conducted on model A at angles of attack to 35° and for flap deflections of 0° and $\pm 50^{\circ}$. Results of the tests are presented in figure 15, wherein lift and pitching-moment coefficient are plotted against dewpoint. The data showed that the aerodynamic coefficients were essentially invariant with dewpoint.

APPENDIX B

EVALUATION OF SUPPORT INTERFERENCE

In order to evaluate the possibility of support interference affecting the data, a limited number of tests were conducted on three preliminary flat-plate models. The models had approximately the same wing area as the wing of model A and the planform was varied to include a circle, a square, and a triangle. The models were constructed from 0.25-inch-thick brass. These flat-plate models were tested in an attitude normal to the free-stream direction in order to simulate a model at 90° angle of attack. Drawings of the disks, illustrating physical dimensions, model designations, and sting locations, are presented in figure 16. A photograph of the models is shown in figure 17(a). Figure 17(b) shows a photograph of the circular model mounted in the tunnel.

Tests were conducted with the flat-plate disks positioned in different longitudinal locations in the wind tunnel and with three different sting attachment points on each disk. (See fig. 16.) By testing in this way, it was possible to alter the structure and the manner in which the wake from each disk intercepted the sting and balance windshield. The resulting effect that this might have on the interference forces could then be determined.

The results of the tests are presented in figure 18 wherein drag coefficient is plotted against sting length for the three sting positions and model shapes. The drag results appear to be sensitive to the value of l, to sting location, and to disk shape. The flagged symbols (for circular and square disks) denote data wherein the pressures on the leeward side of the disk have been measured and used to correct the drag-coefficient values to what they would be if free-stream pressure were acting over the entire leeward side. The data in the plot at the upper left of figure 18 show that when this correction is made the square disk and the circular disk have about the same drag coefficient. This fact indicates that the difference in the data for the disks with different shapes is primarily due to pressures on the leeward side.

It was expected that the variation of drag coefficient with increasing values of l would show no change at large l values; however, for the triangular disk no such constant value is attained. Since sting interference would be expected to increase the disk base pressures, the drag coefficient would be expected to increase with increasing values of l. This is the case for the triangular disk. Although the drag curve for the triangular disk does not become level at large l values, the drag values at the largest l values are believed to be rapidly approaching interference-free values. This belief is strengthened by

the results of a drag estimation. If normal shock pressure is assumed to act on the front of the plate and the base pressure coefficient is assumed to be $-1/M^2$, the resulting drag coefficient is 1.871. If experimental results such as reference 2 are used to predict the base pressure, $C_D = 1.853$. These estimated values are slightly higher than the drag coefficient which is shown at the largest l value but it might be expected that due to edge effects normal shock pressure would not be felt over the entire front face.

The triangular disk at sting location C and $l \approx -0.560$ is the configuration that most nearly corresponds to the geometry of the reentry configuration for which results are presented in the body of the report. Increasing l from 0 to 2.85 inches increased the drag of the disk by 3 percent. This is believed to be representative of the drag error in the test results at $\alpha = 90^\circ$ of the reentry configuration of the body of the report. It is believed that the error is less at lower angles of attack. Figure 4(a) (model A without flaps) shows a drag-coefficient value for the reentry configuration at $\alpha = 90^\circ$ of $C_D = 1.58$. This is far below the value measured on the triangular disk. However, the triangular disk had a square-cornered leading edge and the reentry configuration had a hemicylindrically blunted leading edge. The drag-coefficient increment due to rounding the leading edge was computed by use of Newtonian theory and was found to be $\Delta C_D = -0.060$. This incremental-drag-coefficient value has been subtracted from each of the values of drag coefficient for the triangular disk tested in sting location C and is presented as the dashed curve (lower right) in figure 18. This correction partially accounts for the lower value of drag coefficient on the reentry configuration ($C_D = 1.58$) as compared to that for the triangular disk. The discrepancy between the dashed curve and $C_D = 1.58$ can probably be attributed to a combination of differences in base pressures acting on the two different configurations and in model support interference.

In summary, it is believed that the 3-percent variation in drag for the triangular disk between $l = 0$ and $l = 2.85$ inches is representative of the error in the drag-coefficient results of the reentry configuration near $\alpha = 90^\circ$. At lower angles of attack the error is believed to be less.

REFERENCES

1. Rainey, Robert W.: Investigation of the Effects of Bomb-Bay Configuration Upon the Aerodynamic Characteristics of a Body With Circular Cross Section at Supersonic Speeds. NACA RM L55E27, 1955.

2. Love, Eugene S.: Base Pressure at Supersonic Speeds on Two-Dimensional Airfoils and on Bodies of Revolution With and Without Fins Having Turbulent Boundary Layers. NACA TN 3819, 1957. (Supersedes NACA RM L53C02.)

TABLE I.- GEOMETRIC PROPERTIES OF MODELS

Description	Model A	Model B	Model C	Model D
Wing span, in.	2.460	2.443	3.179	3.179
Wing mean aerodynamic chord, in.	3.271	3.275	4.170	4.155
Wing area, sq in.:				
Rectangular holes open	5.875	5.770	9.539	9.502
Rectangular holes covered	6.401	-----	-----	-----
Wing thickness ratio, percent	3.13	1.57	3.97	4.00
Aspect ratio	1.030	1.034	1.056	1.064
Sweep of wing leading edge, deg	75	75	75	75
Flap area, sq in.	0.212	0.212	0.406	0.406
Tip-fin area, sq in.	0.400(small) 0.900(large)	0.224	0.441	0.441

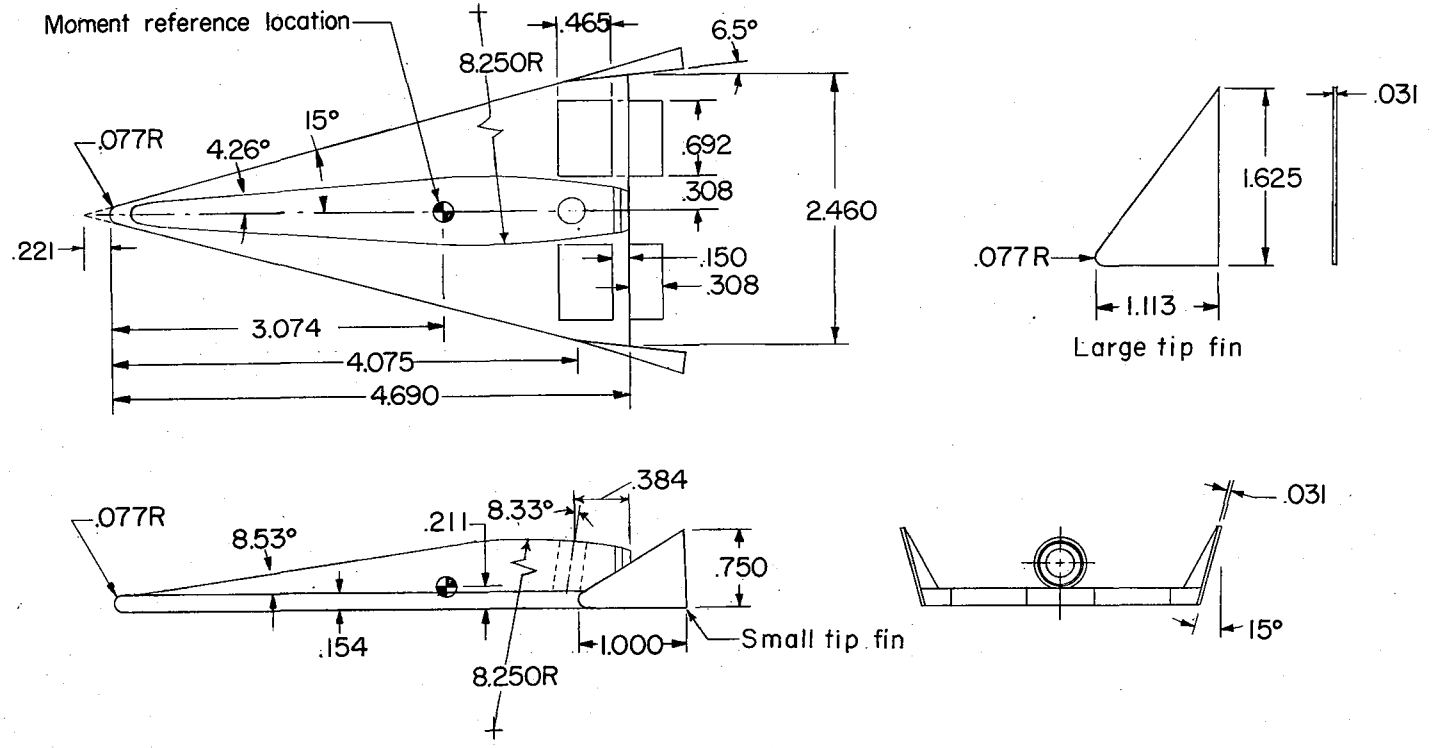

(a) Model A.

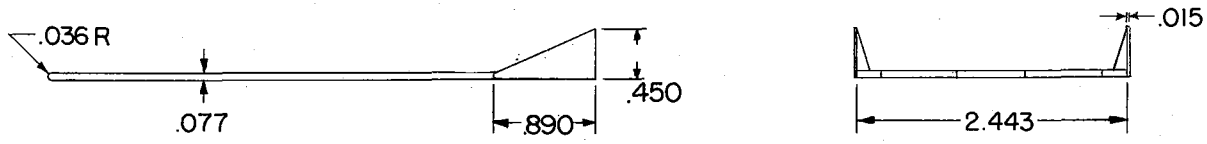

(b) Model B.

Figure 1.- Three-view drawing of models. All dimensions are in inches.

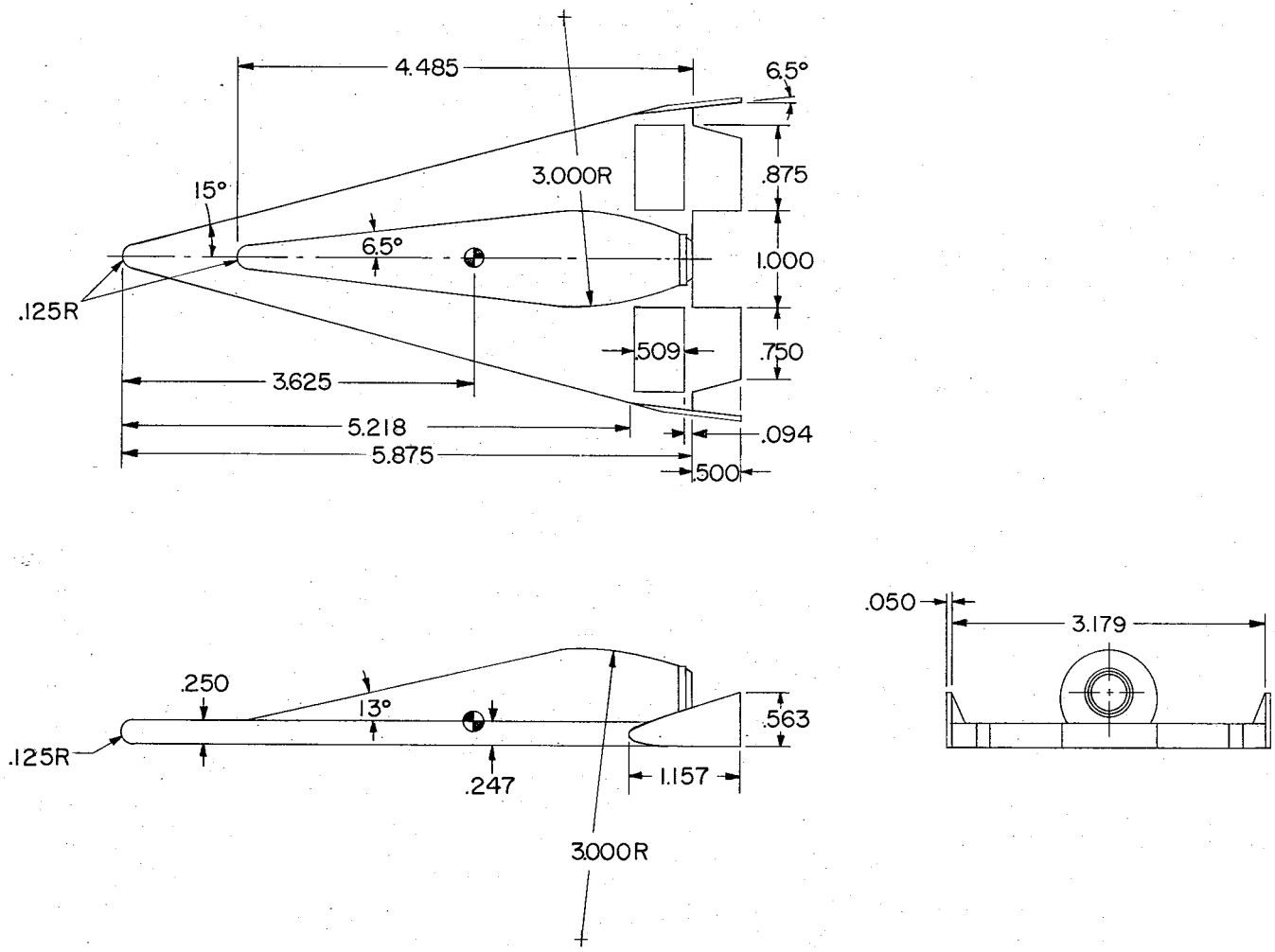

(c) Model C.

Figure 1.- Continued.

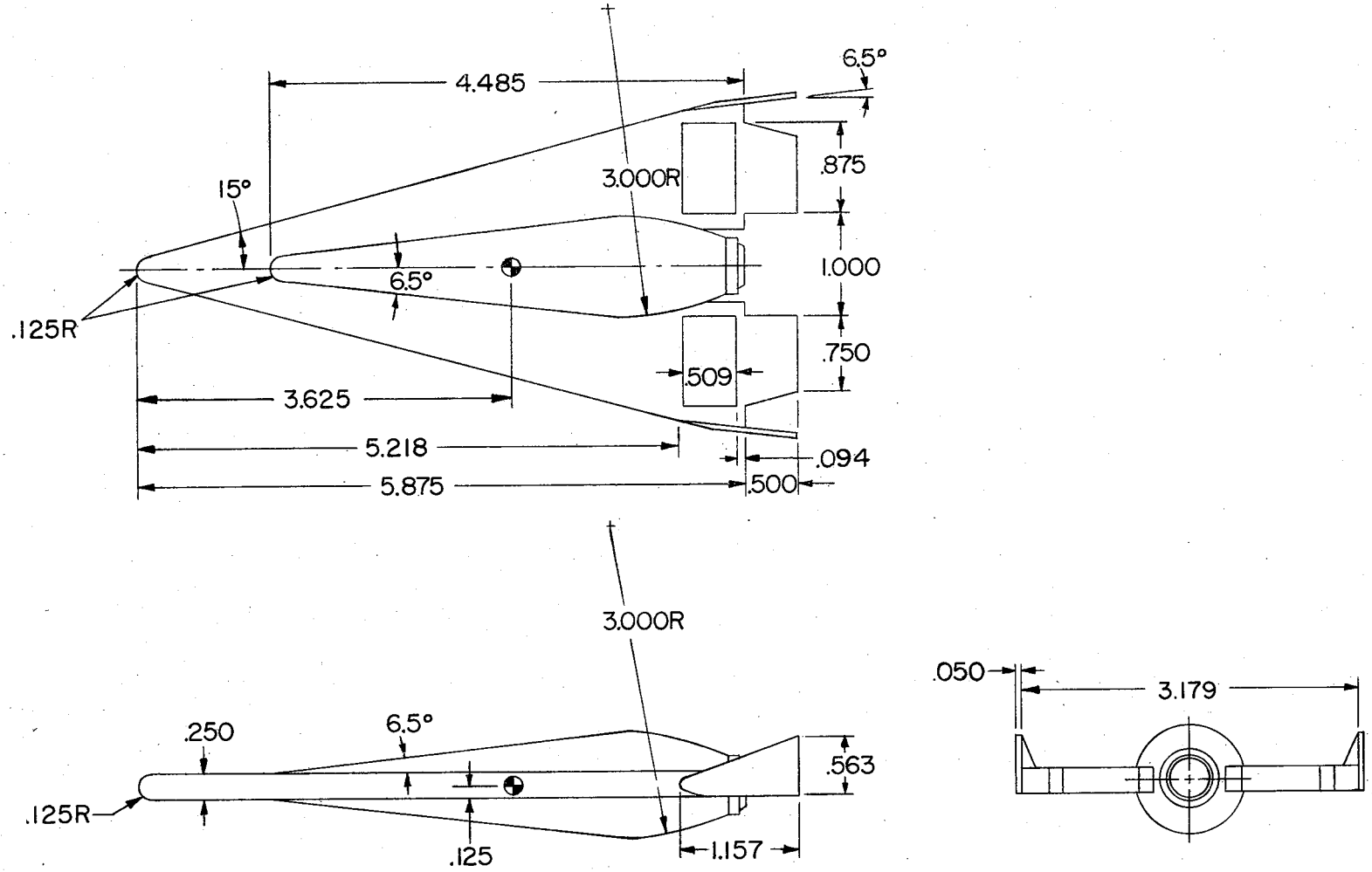

(d) Model D.

Figure 1.- Concluded.

CONFIDENTIAL

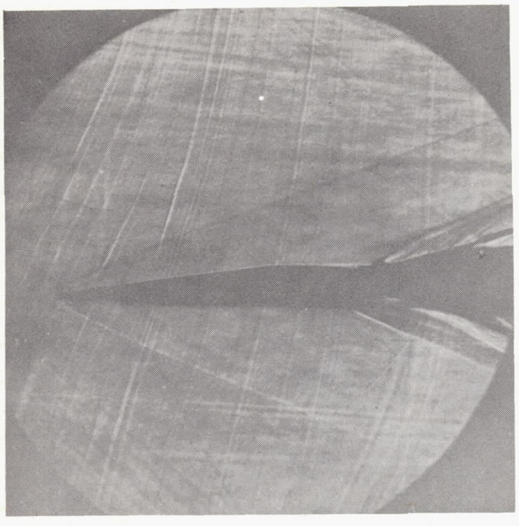

$\alpha = 0°$

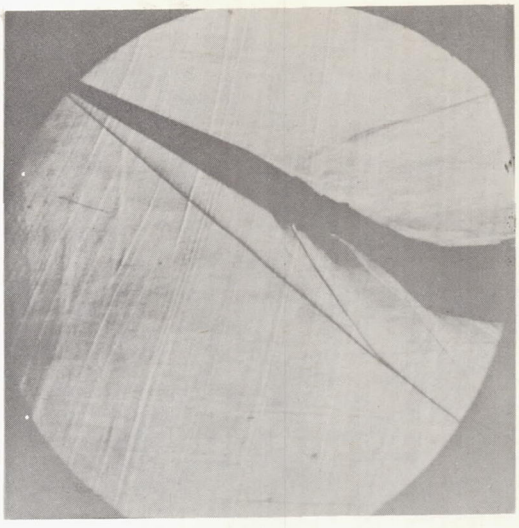

$\alpha = 30°$

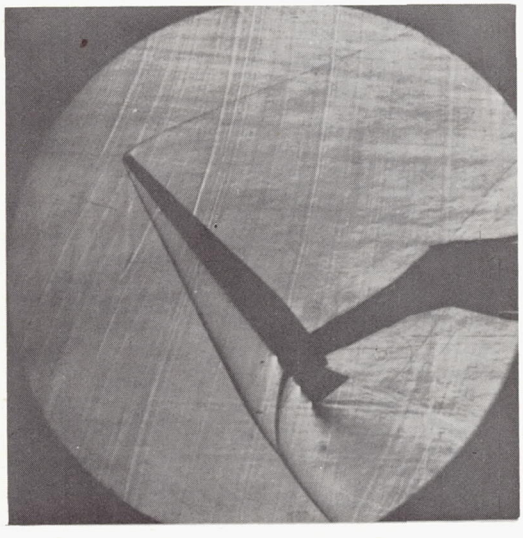

$\alpha = 50°$

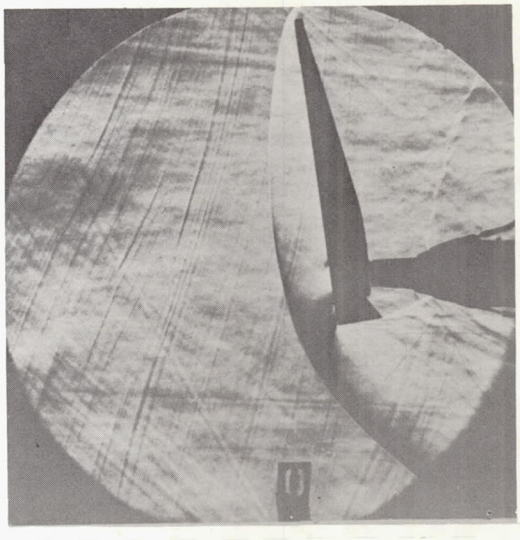

$\alpha = 81°$

L-60-2500

Figure 2.- Typical schlieren photographs of model A at various angles of attack.

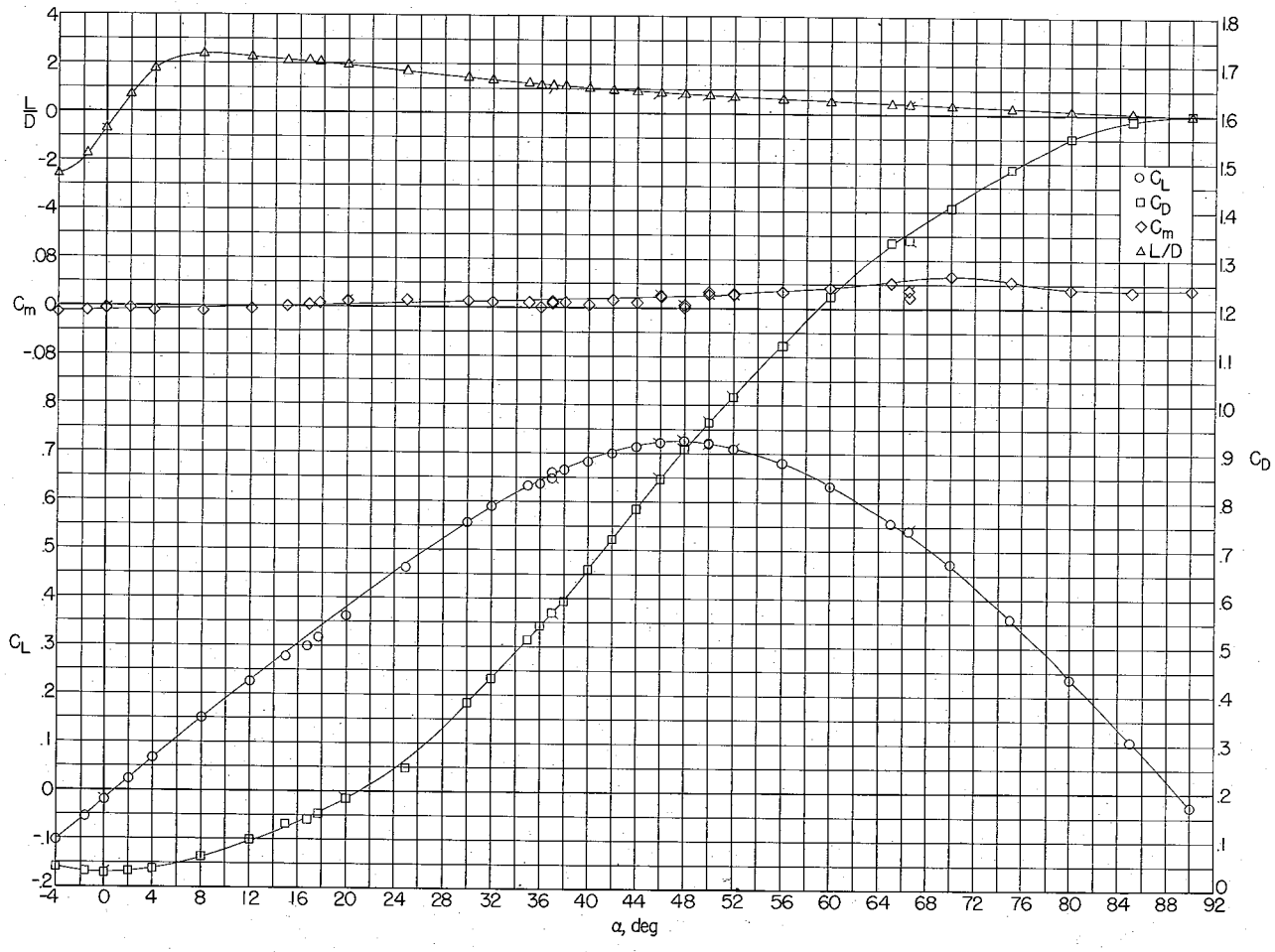

(a) Without flaps.

Figure 3.- Variation of C_L, C_D, C_m, and L/D with angle of attack for model A (rectangular holes opened). (Flagged symbols denote check points.)

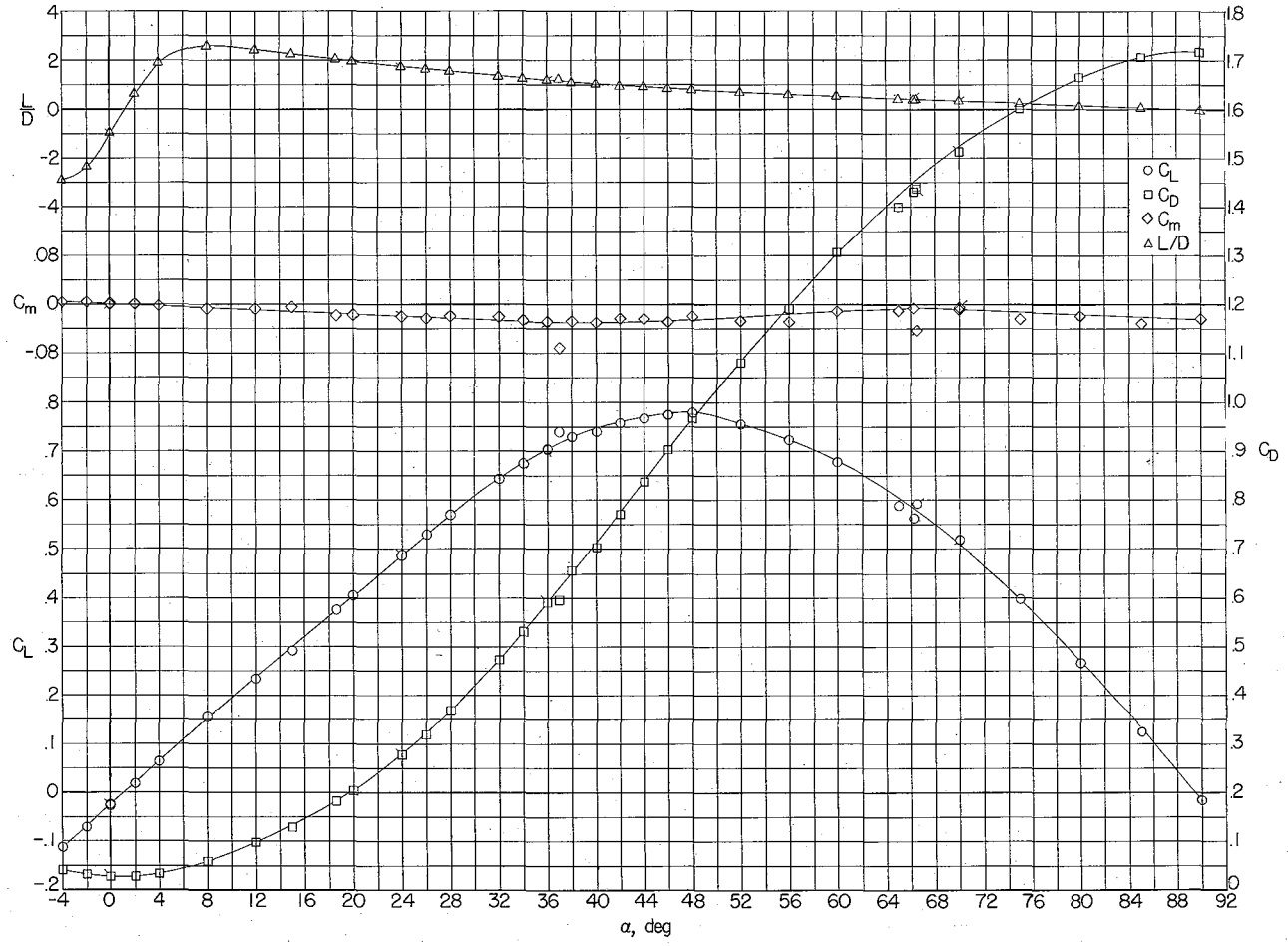

(b) $\delta = 0^\circ$.

Figure 3.- Continued.

CONFIDENTIAL

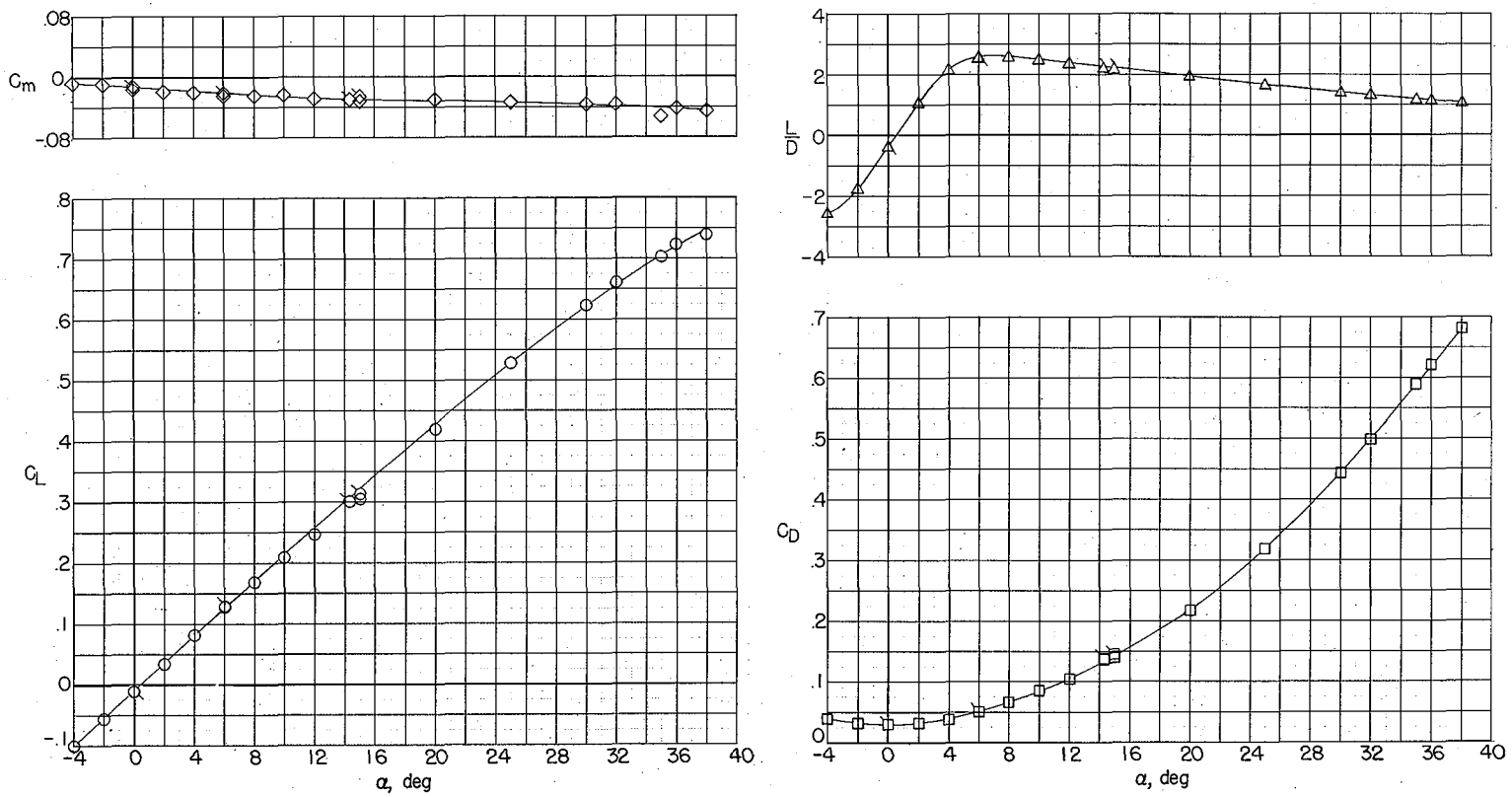

(c) $\delta = 10^{\circ}$.

Figure 3.- Continued.

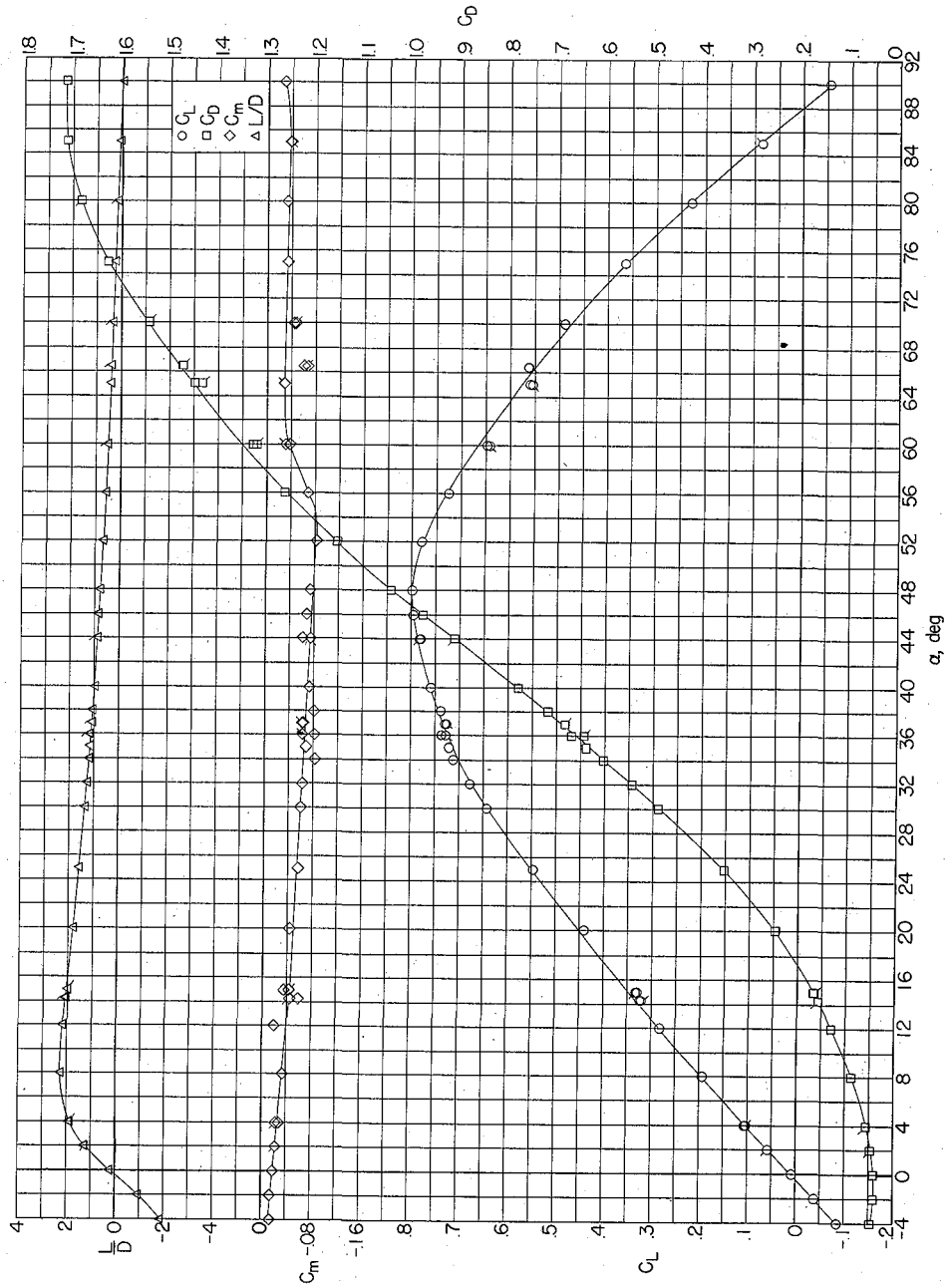

(d) $\delta = 20^{\circ}$.

Figure 3.- Continued.

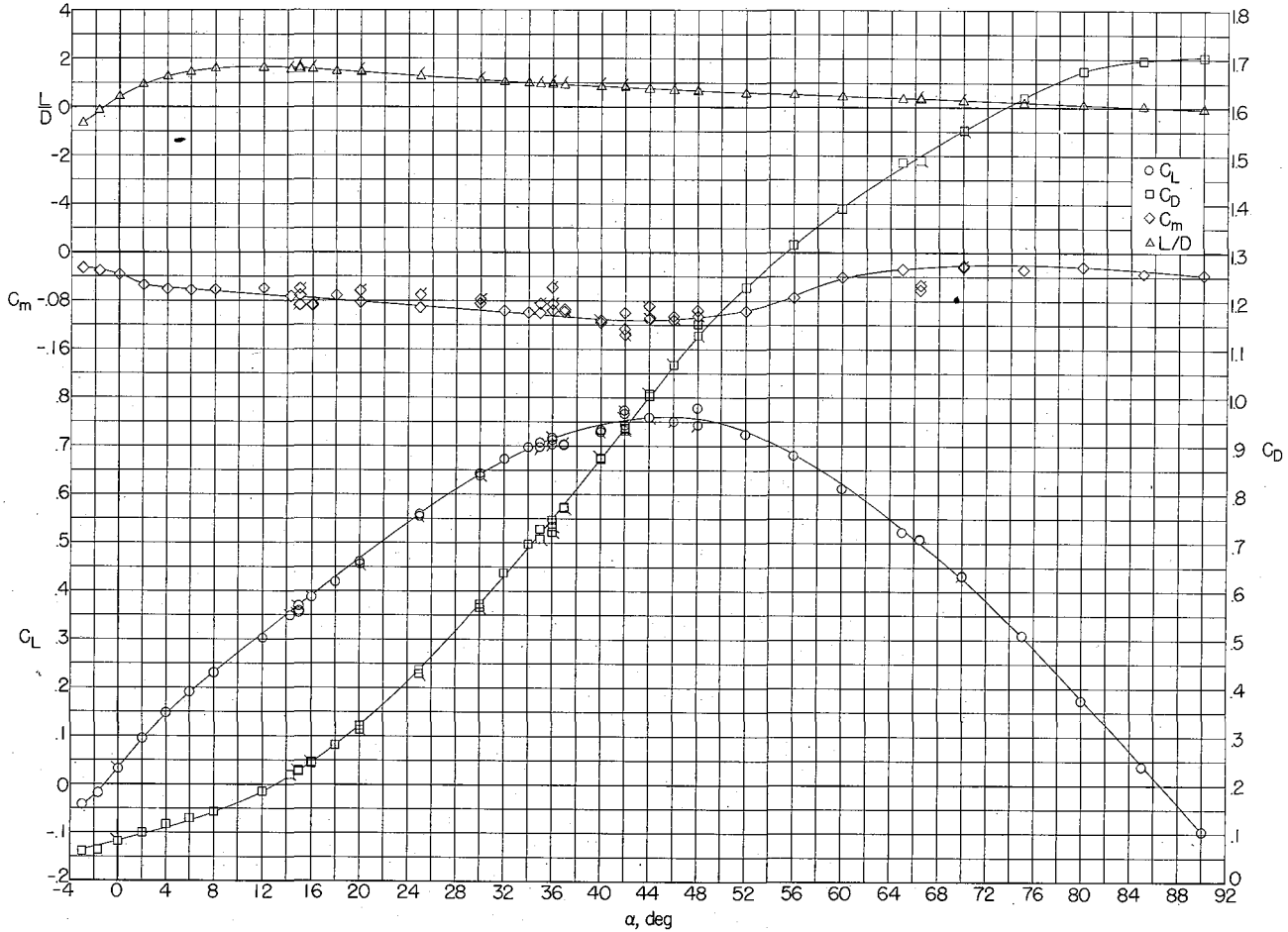

(e) $\delta = 50^{\circ}$.

Figure 3.- Continued.

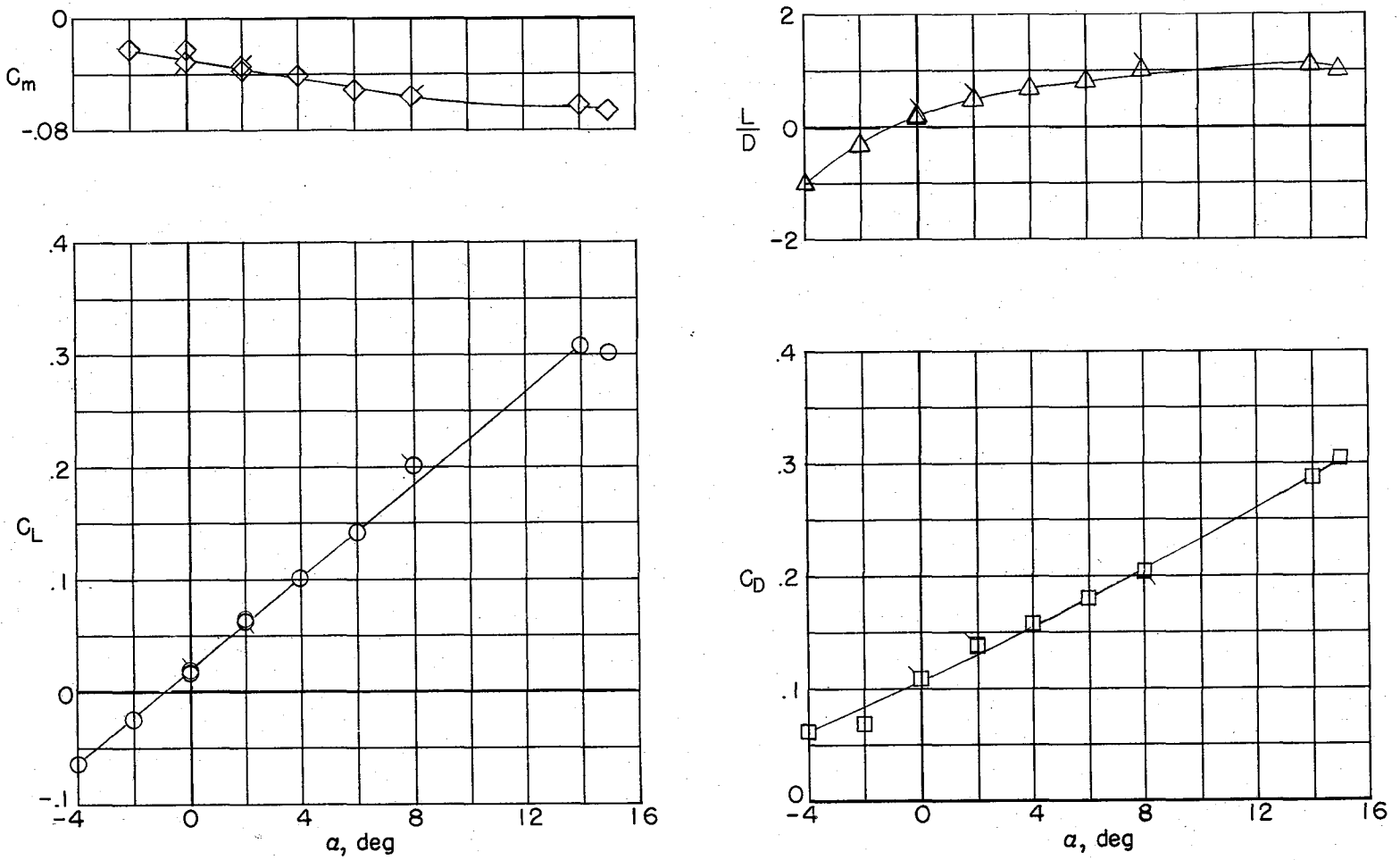

(f) $\delta = 90^{\circ}$.

Figure 3.- Continued.

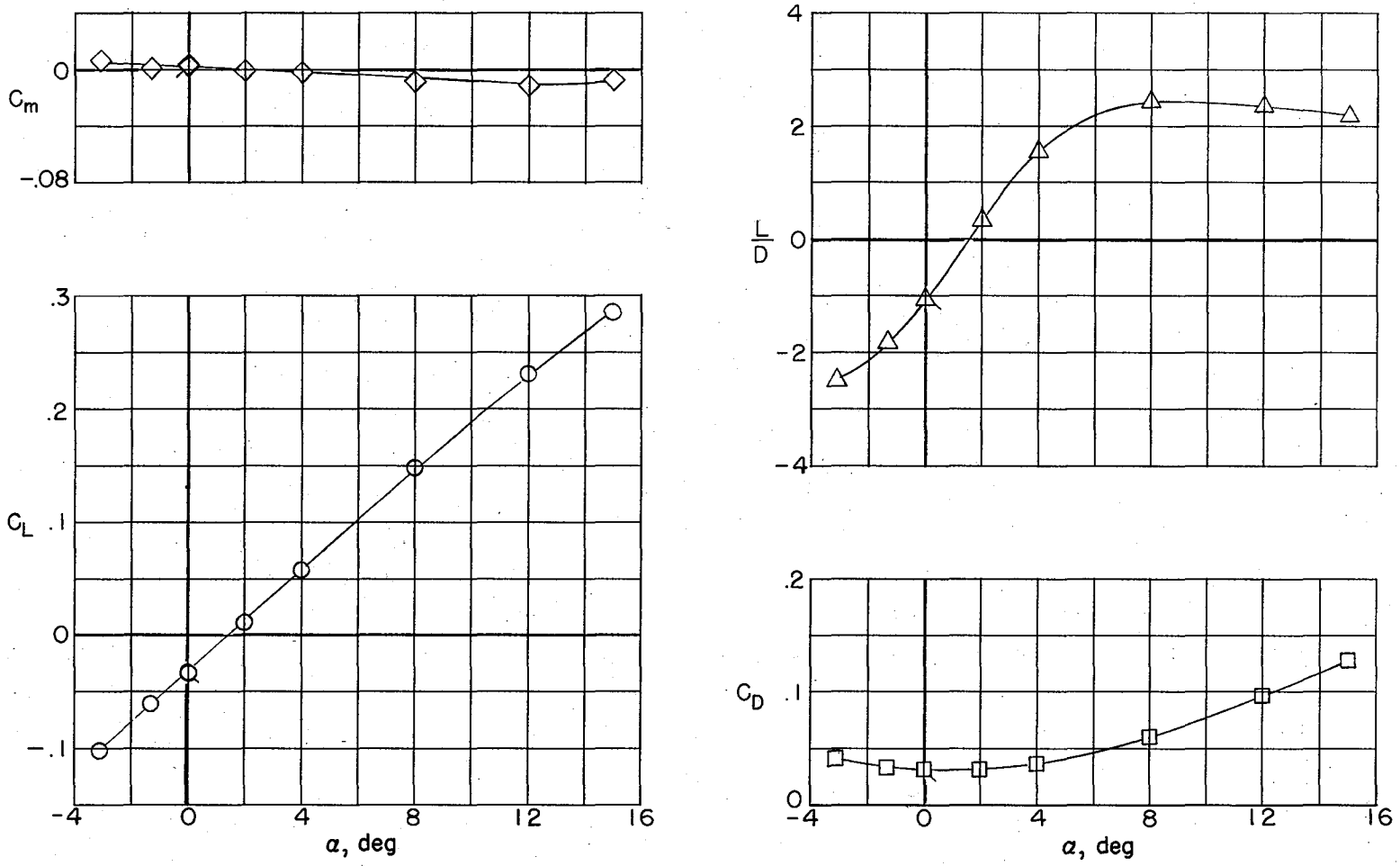

(g) $\delta = -10^{\circ}$.

Figure 3.- Continued.

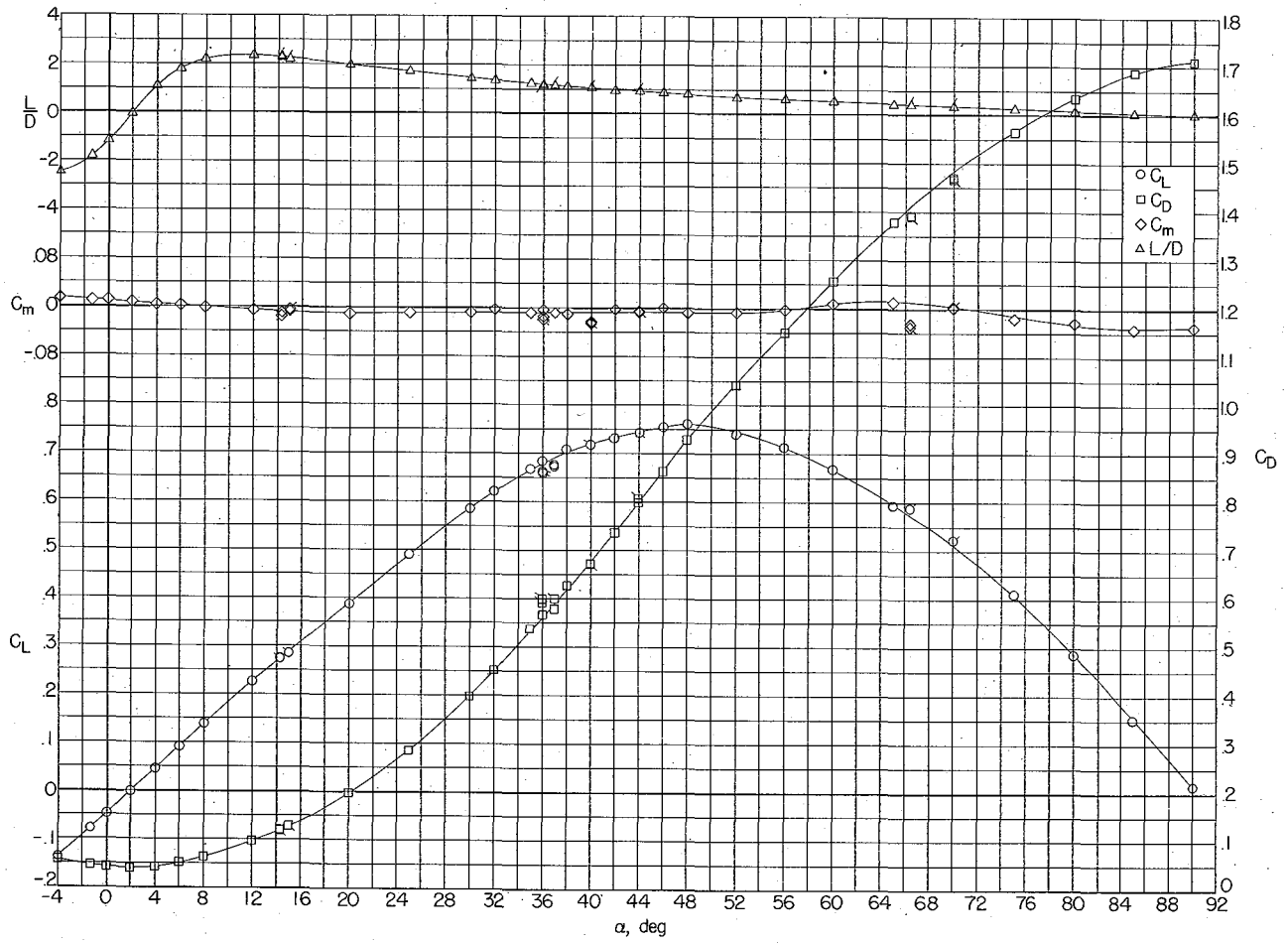

(h) $\delta = -20^{\circ}$.

Figure 3.- Continued.

CONFIDENTIAL

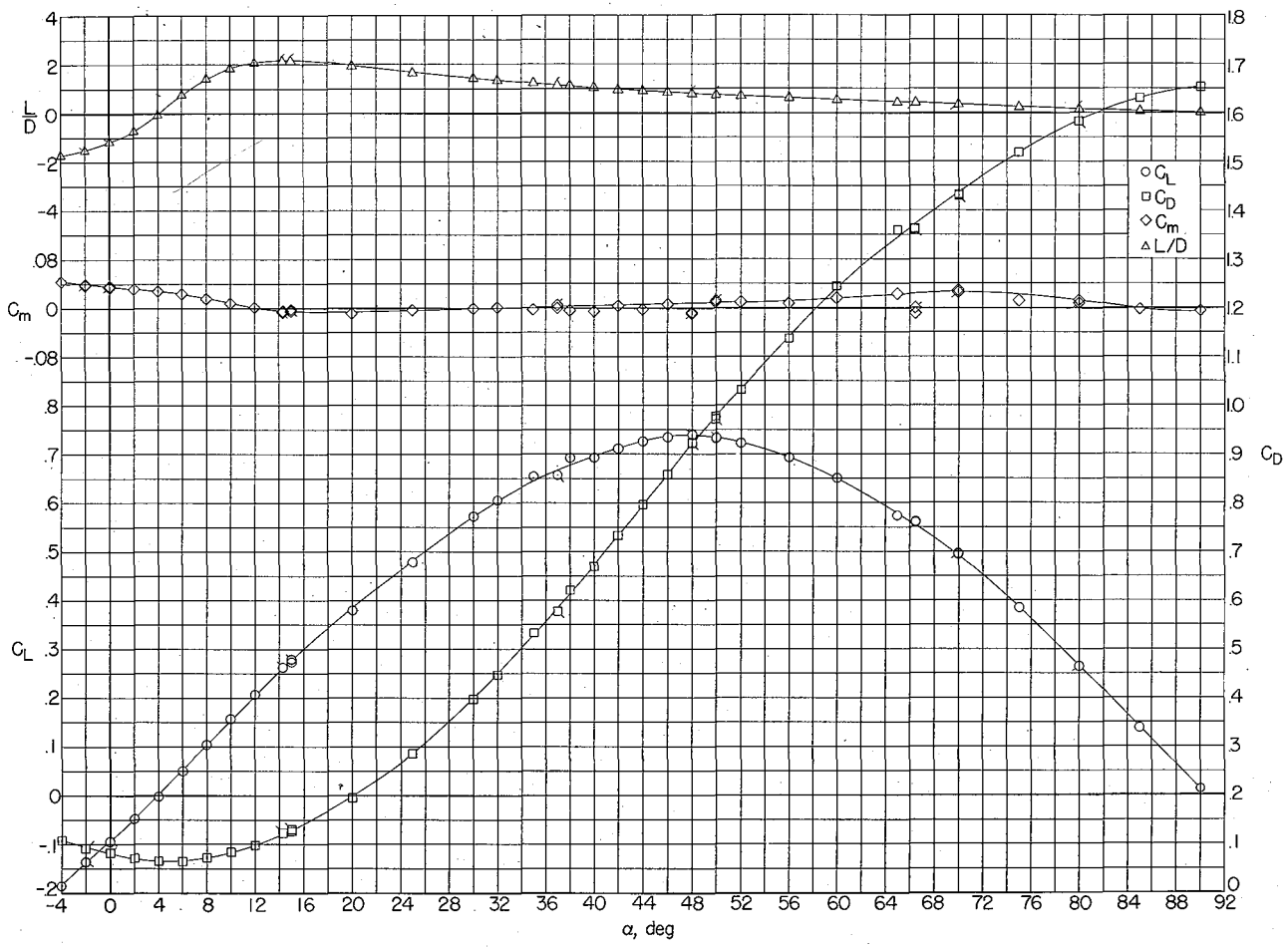

(i) $\delta = -50^{\circ}$.

Figure 3.- Continued.

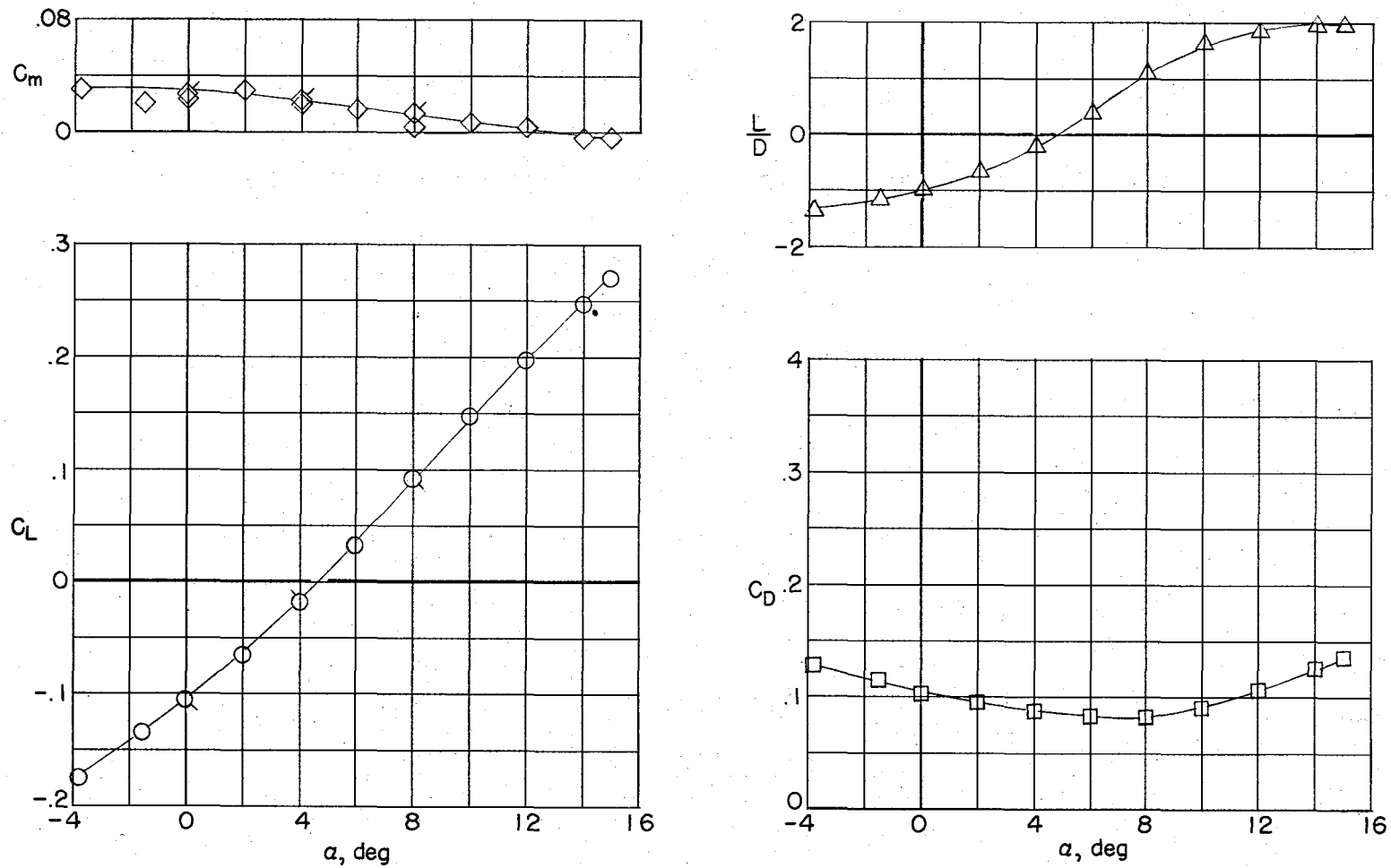

(j) $\delta = -90^{\circ}$.

Figure 3.- Concluded.

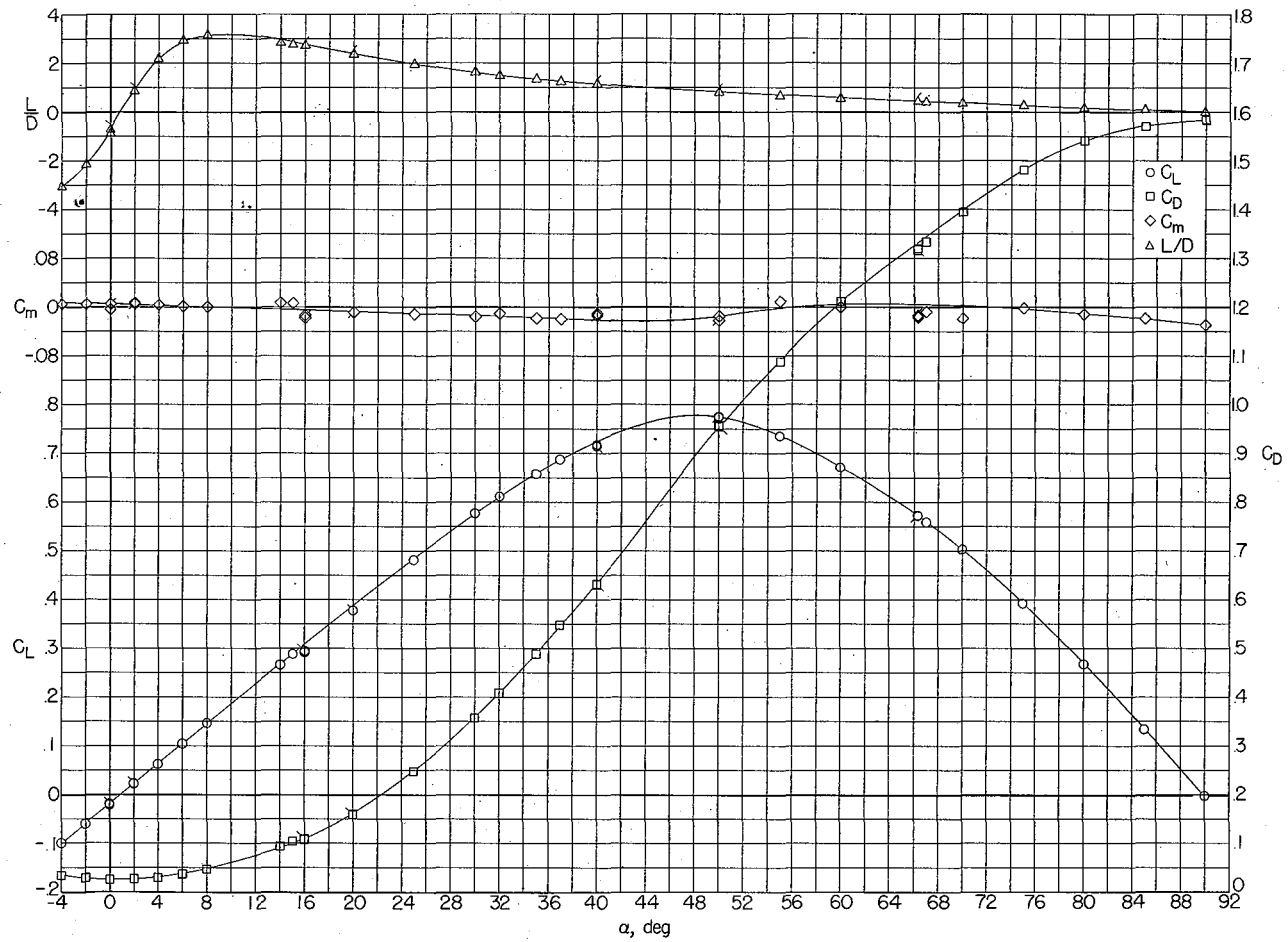

(a) Without flaps.

Figure 4.- Variation of C_L, C_D, C_m, and L/D with angle of attack for model A (rectangular holes covered). (Flagged symbols denote check points.)

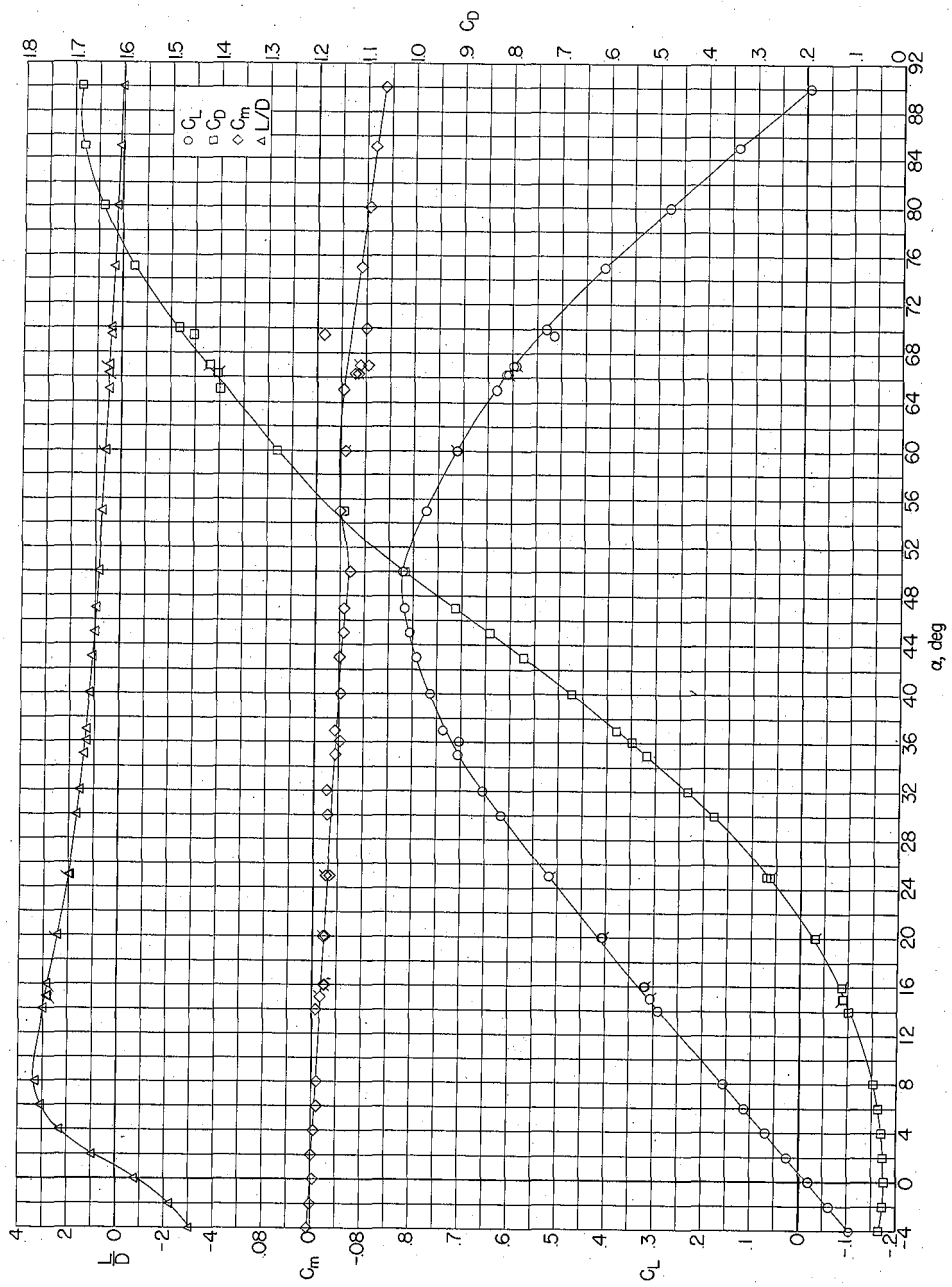

(b) $\delta = 0^\circ$.

Figure 4.- Continued.

(c) $\delta = 20^{\circ}$.

Figure 4.- Continued.

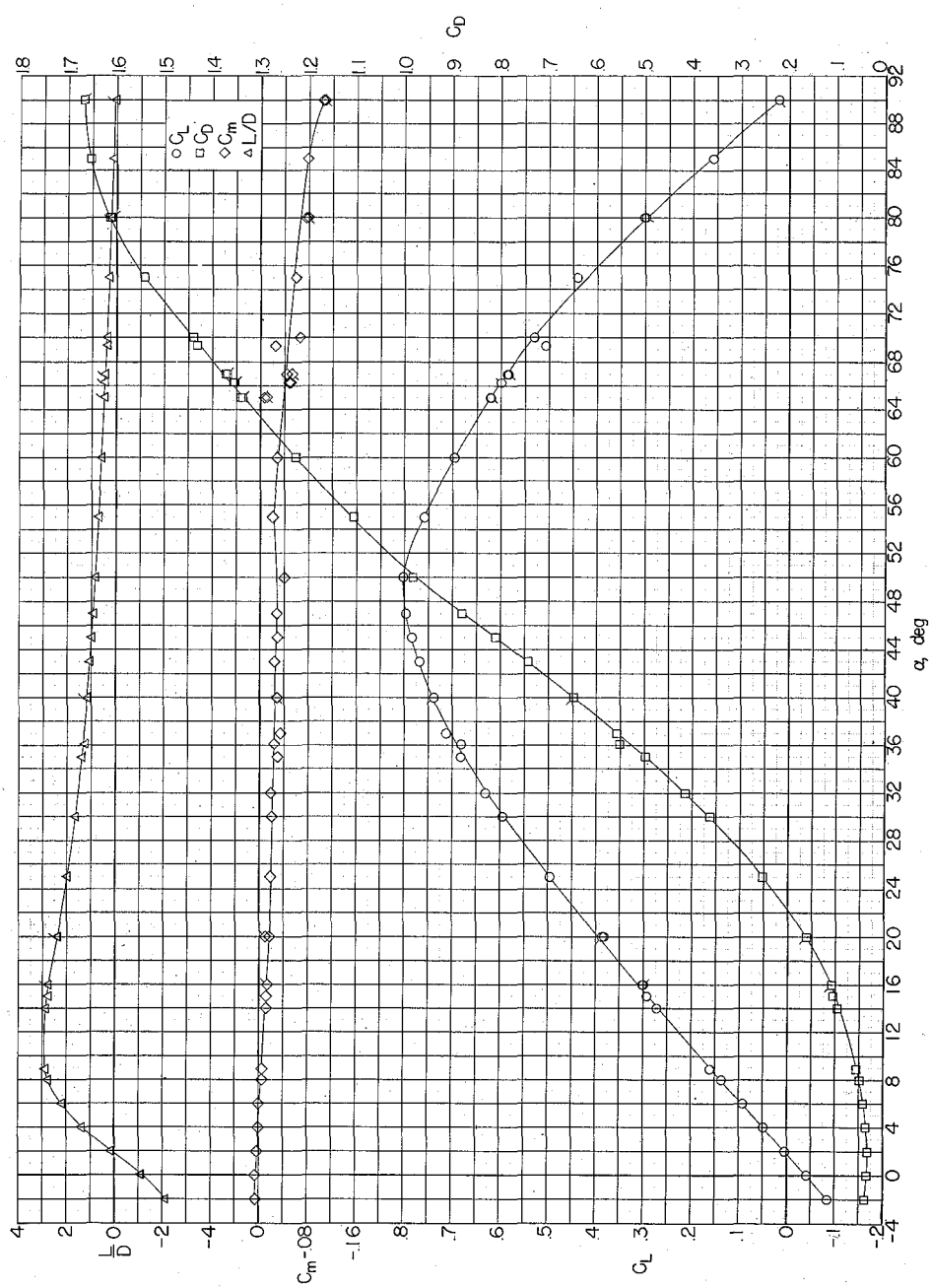

(d) $\delta = -20^{\circ}$.

Figure 4.- Concluded.

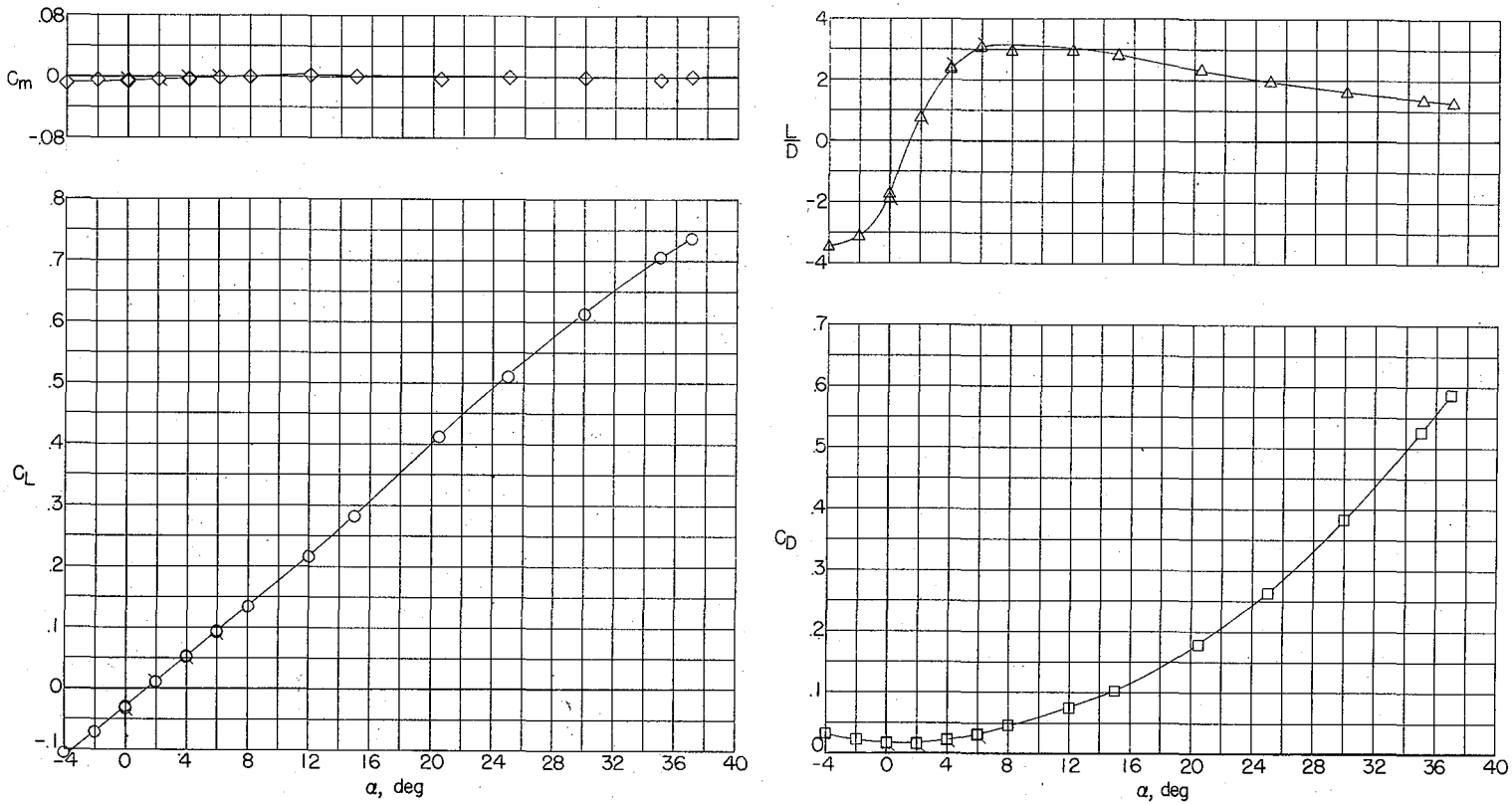

(a) $\delta = 0^{\circ}$.

Figure 5.- Variation of C_L, C_D, C_m, and L/D with angle of attack for model B (rectangular holes opened). (Flagged symbols denote check points.)

CONFIDENTIAL

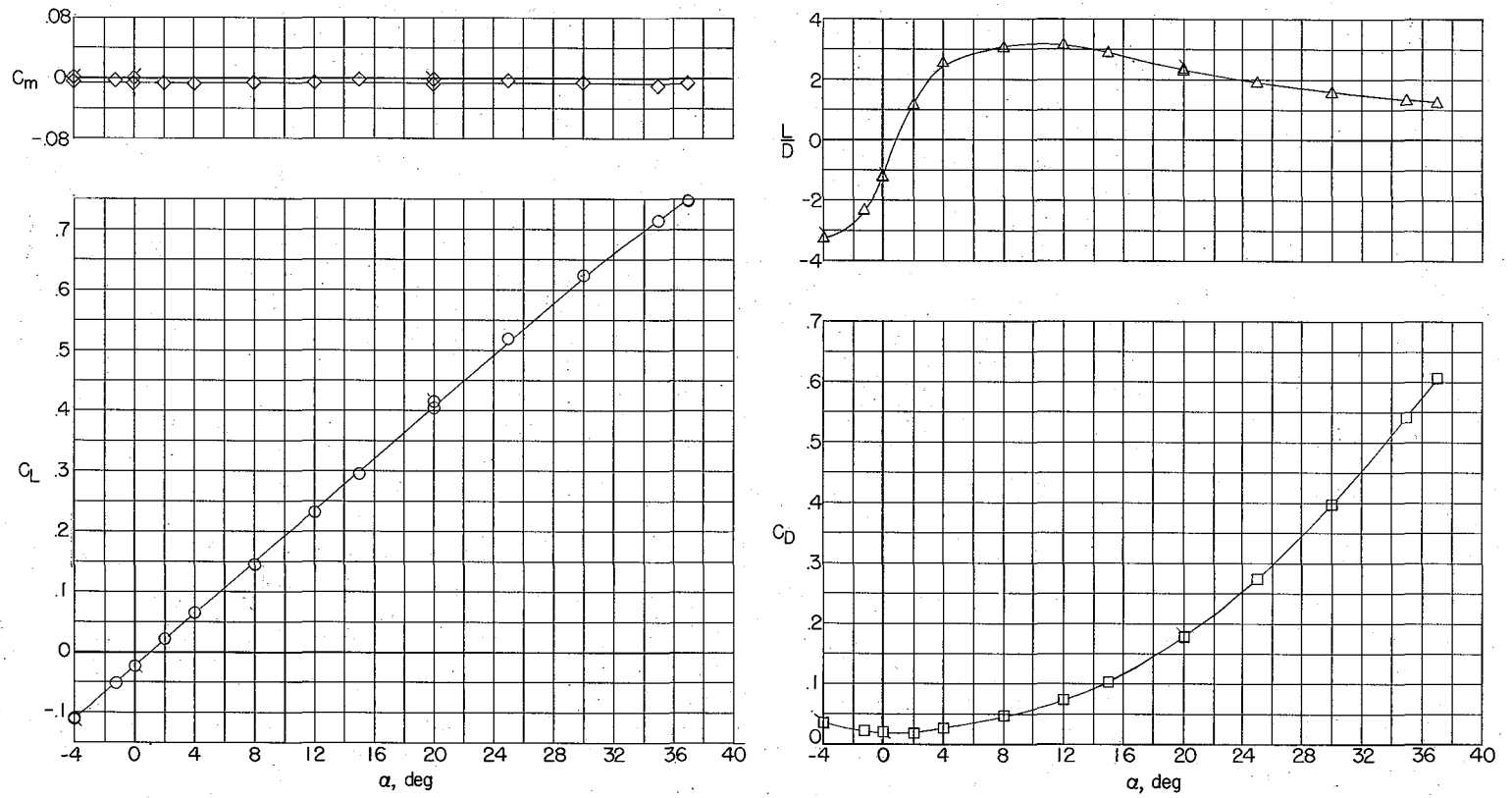

(b) $\delta = 5^{\circ}$.

Figure 5.- Concluded.

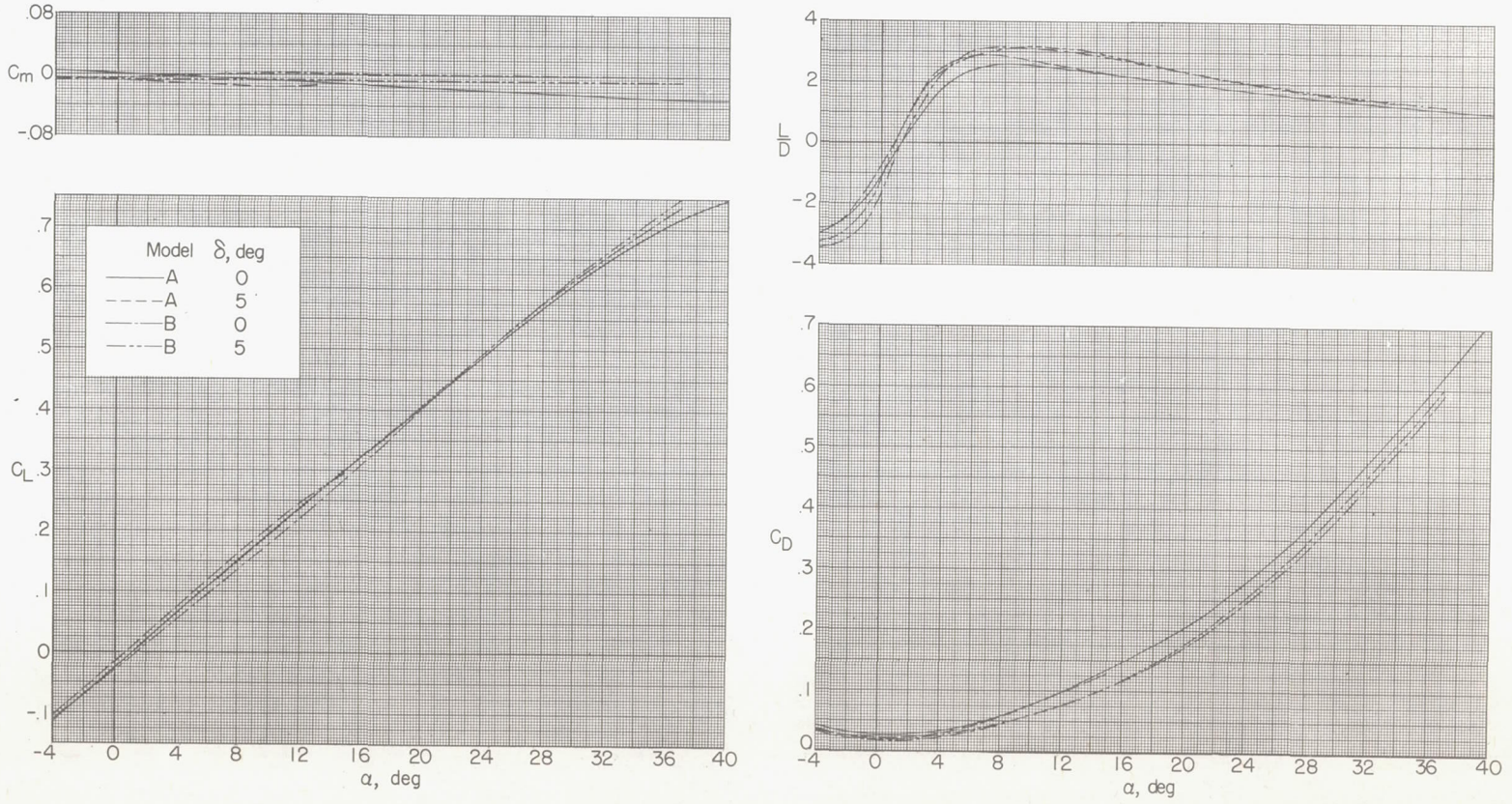

Figure 6.- Comparison of C_L, C_D, C_m, and L/D with angle of attack for model A and model B (rectangular holes opened).

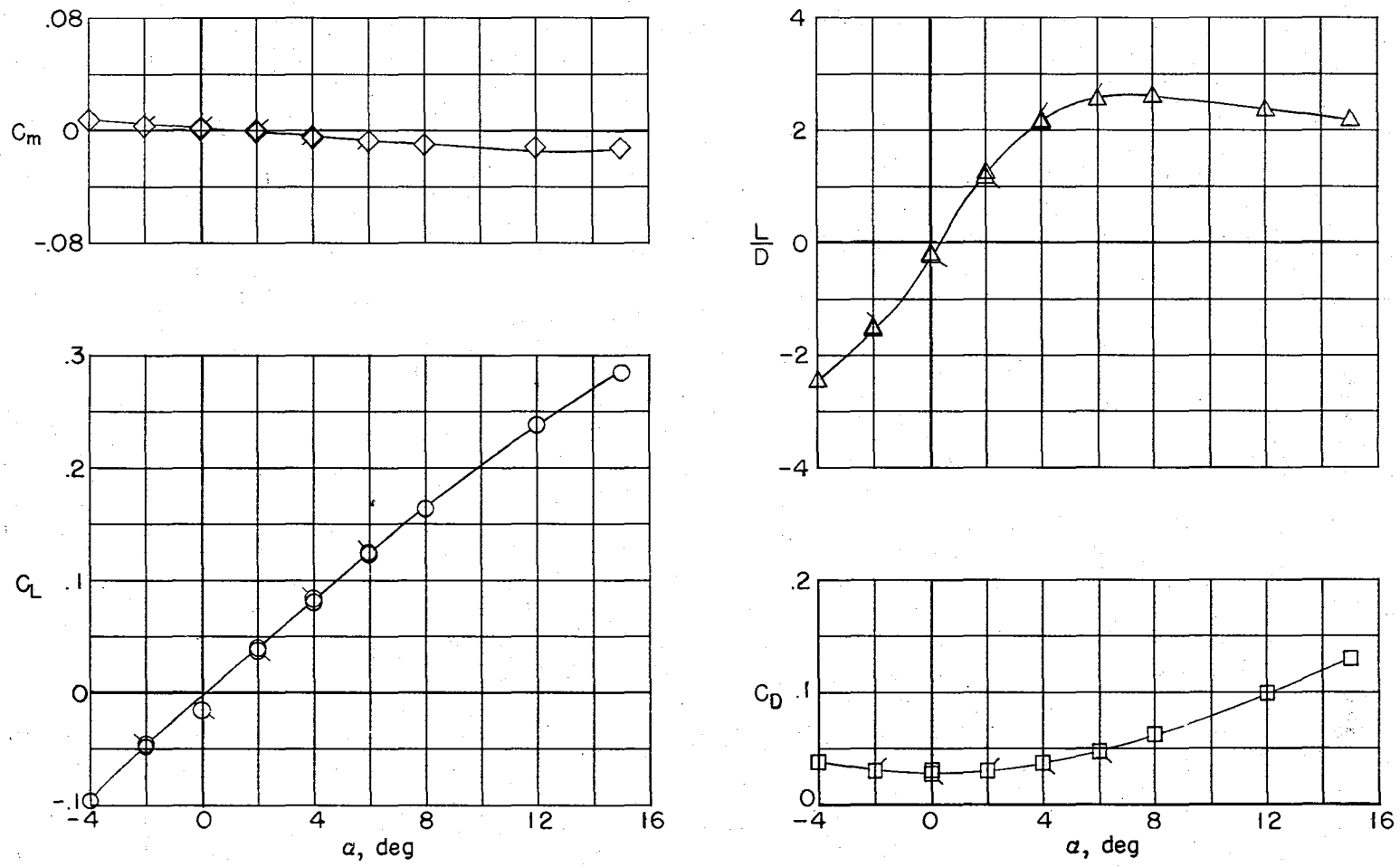

Figure 7.- Variation of C_L, C_D, C_m, and L/D with angle of attack for model C (rectangular holes opened). (Flagged symbols denote check points.)

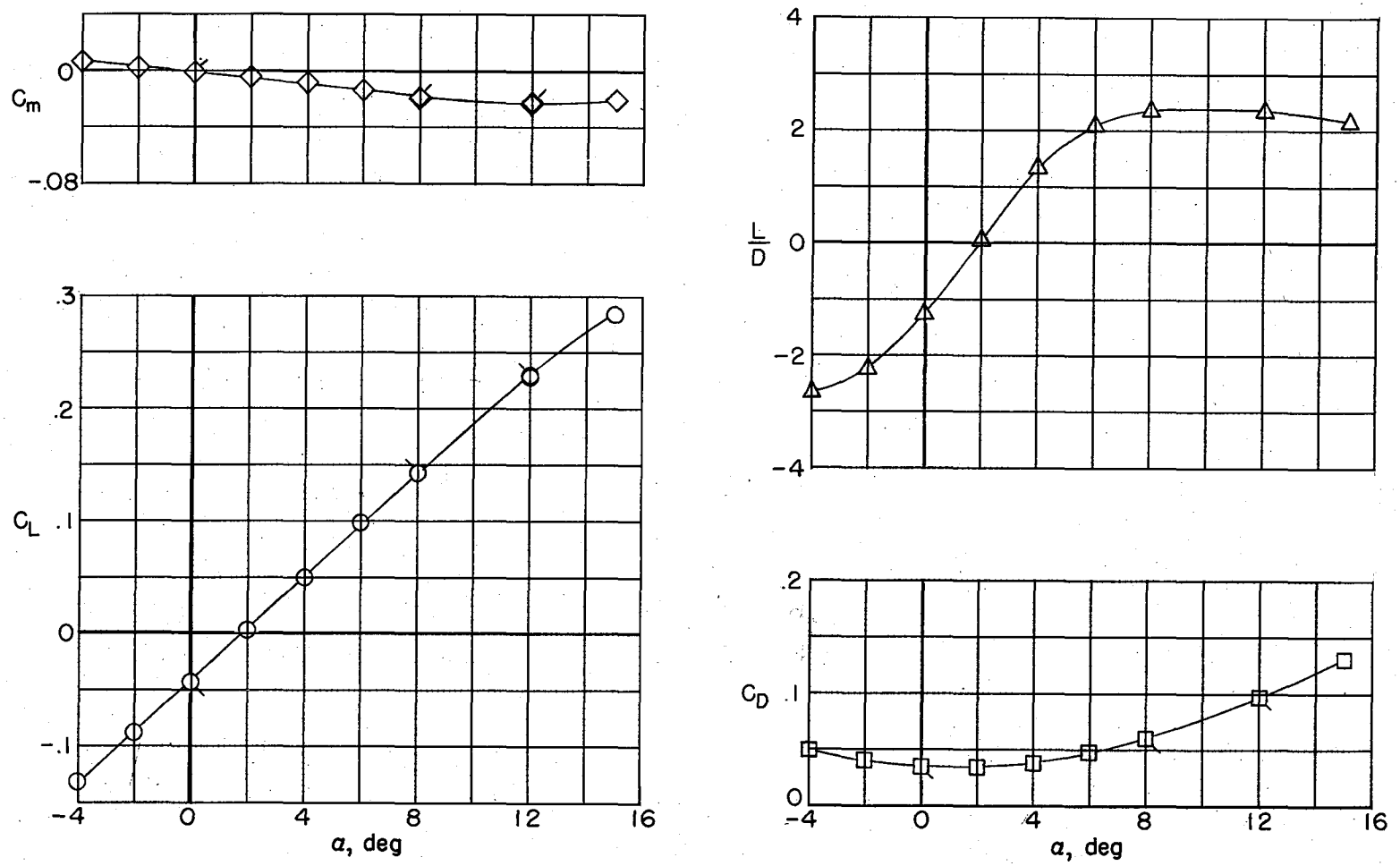

Figure 8.- Variation of C_L, C_D, C_m, and L/D with angle of attack for model D (rectangular holes opened). (Flagged symbols denote check points.)

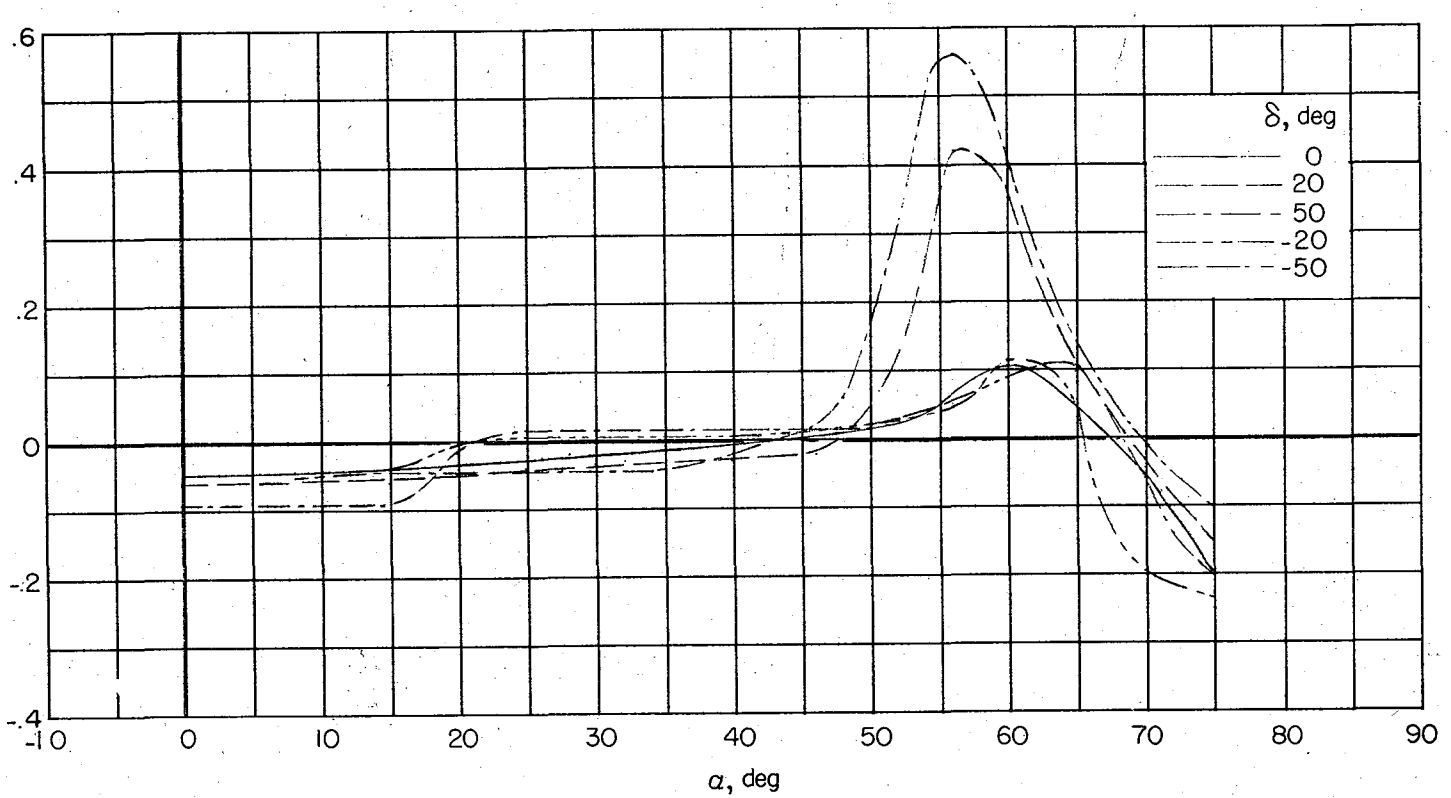

Figure 9.- Variation of aerodynamic-center location with angle of attack for model A (rectangular holes opened).

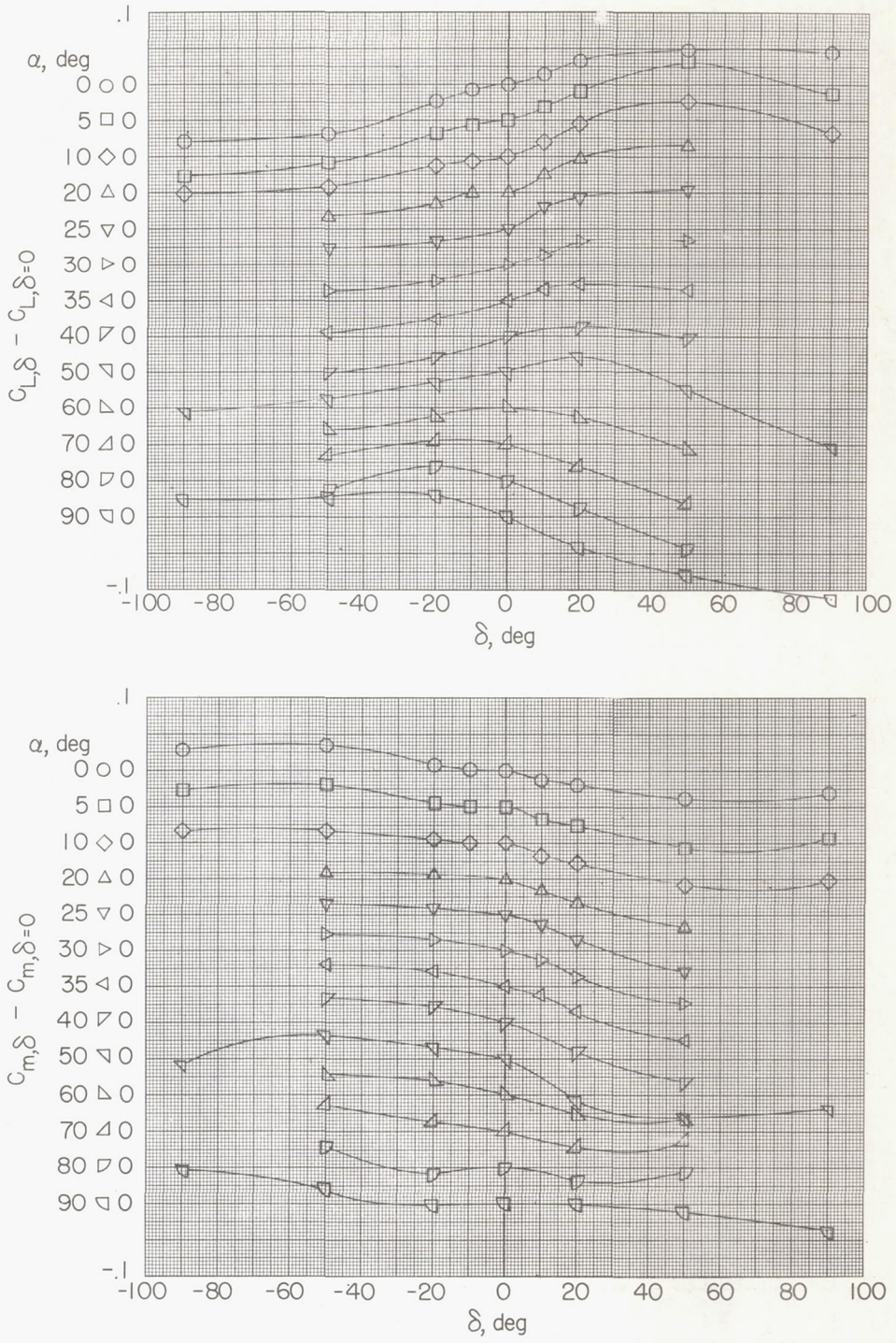

Figure 10.- Variation of incremental value of C_L and C_m with flap deflection for model A (rectangular holes opened).

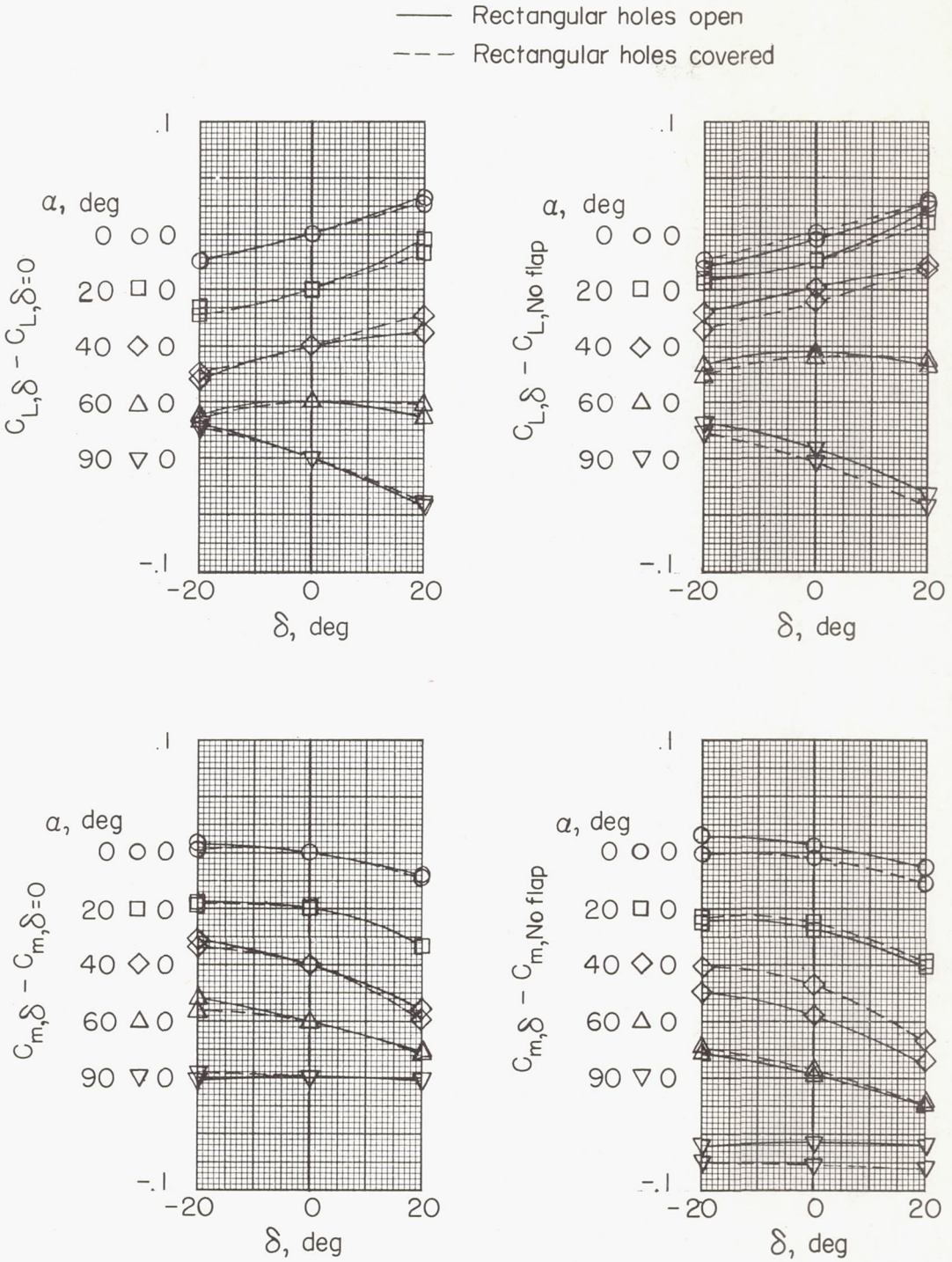

Figure 11.- Variation of incremental value of C_L and C_m with flap deflection for model A (rectangular holes opened and covered).

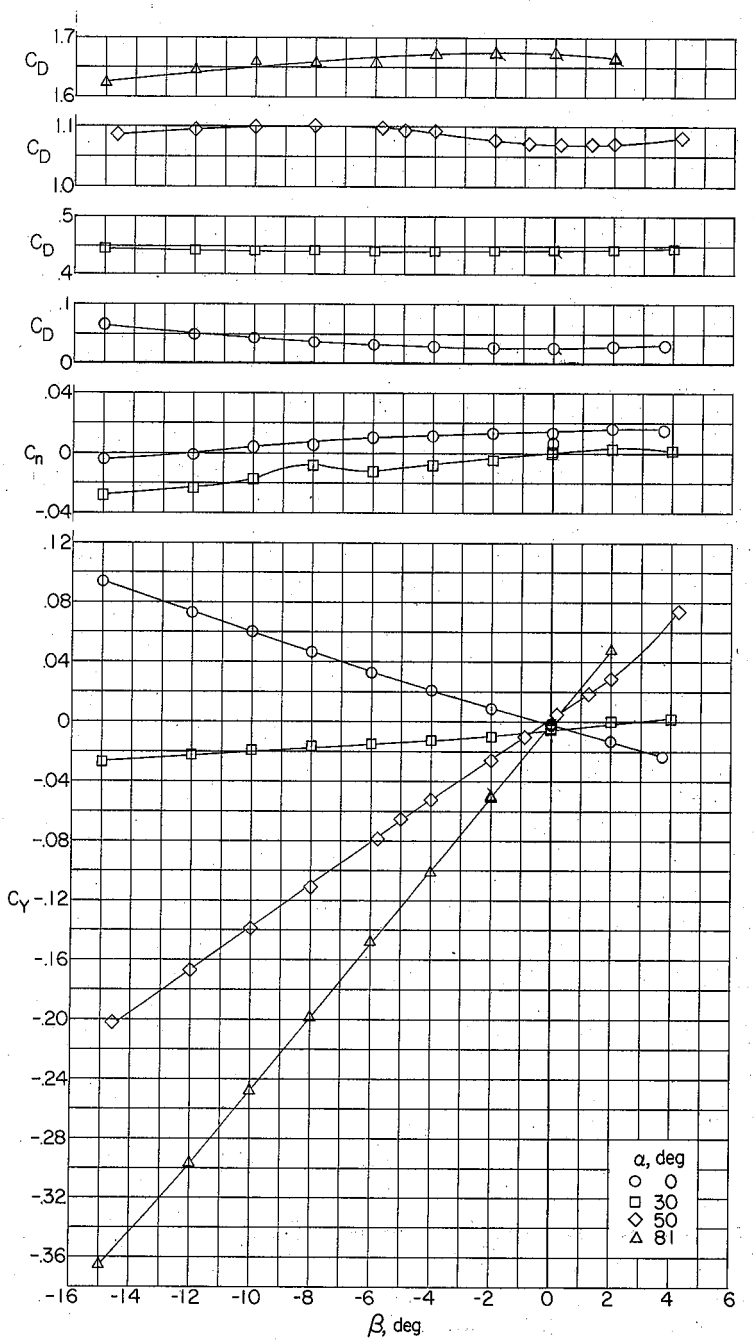

Figure 12.- Variation of C_D, C_Y, and C_n with angle of sideslip for various angles of attack for model A. Small tip fins canted outward; $\delta = 0^o$. (Flagged symbols denote check points.)

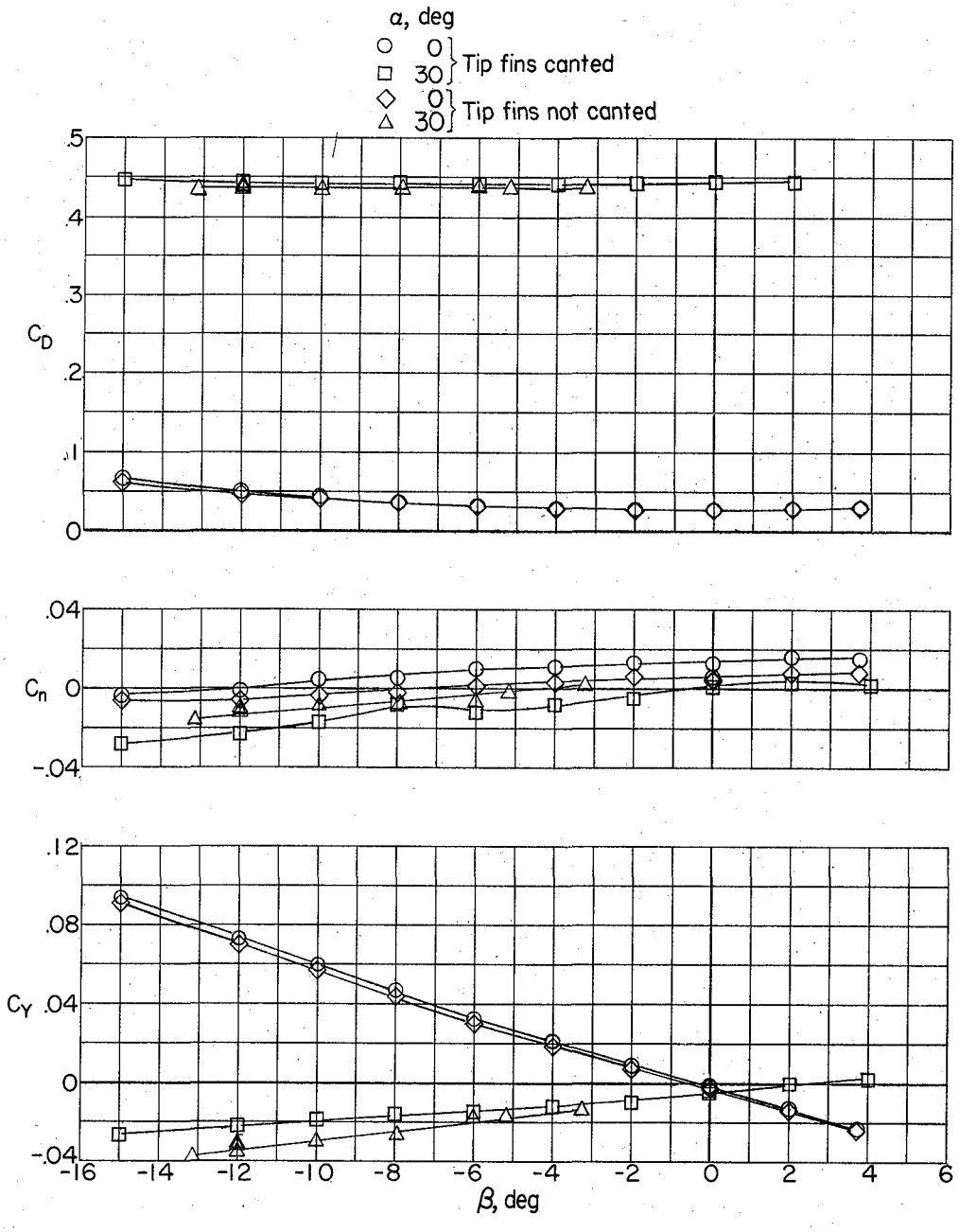

Figure 13.- Variation of C_D, C_Y, and C_n with angle of sideslip for various angles of attack for model A. Small tip fins canted and not canted; $\delta = 0^\circ$.

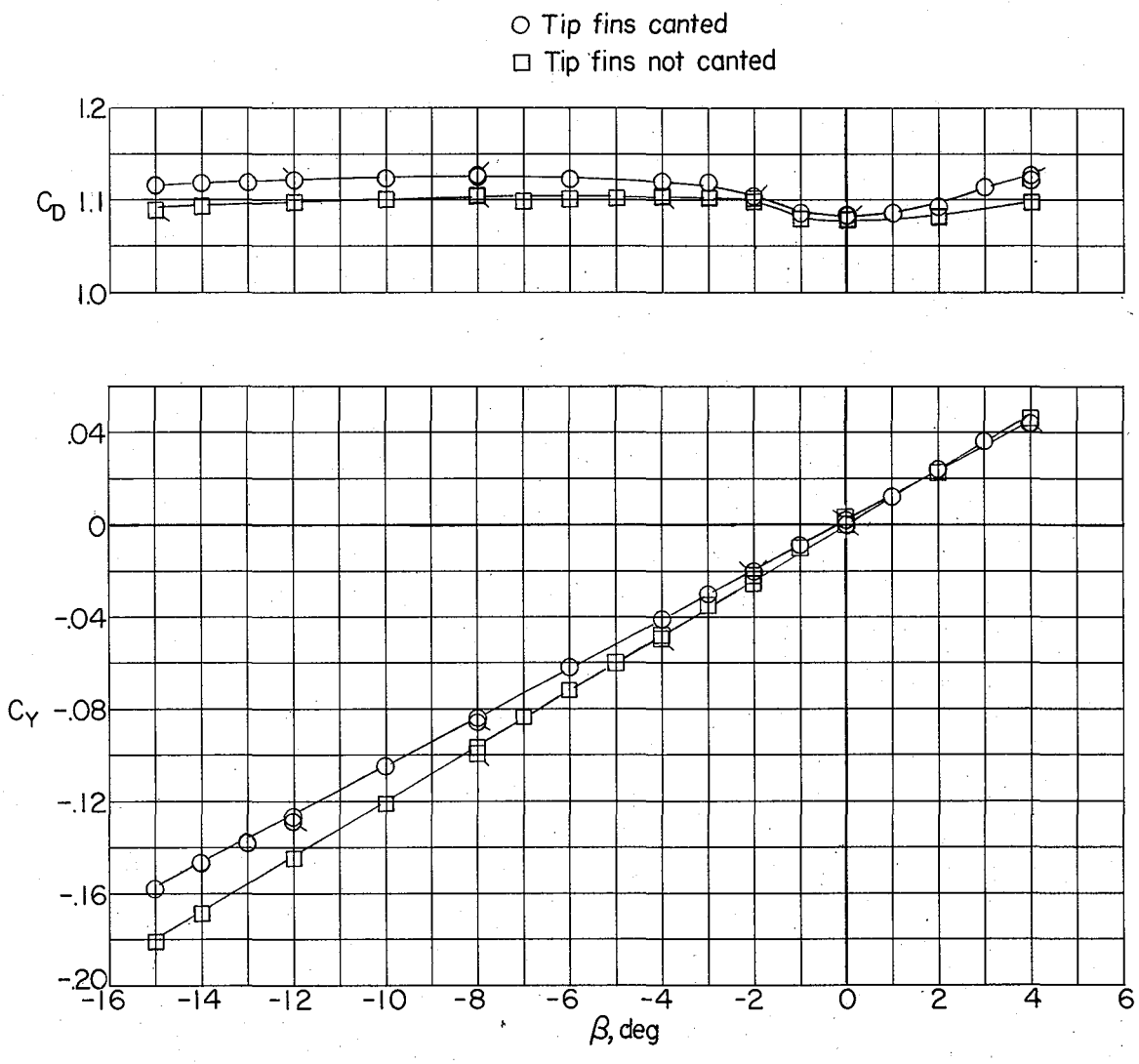

Figure 14.- Variation of C_D and C_Y with angle of sideslip for angle of attack of 50° for model A. Large tip fins canted and not canted; $\delta = 0°$. (Flagged symbols denote check points.)

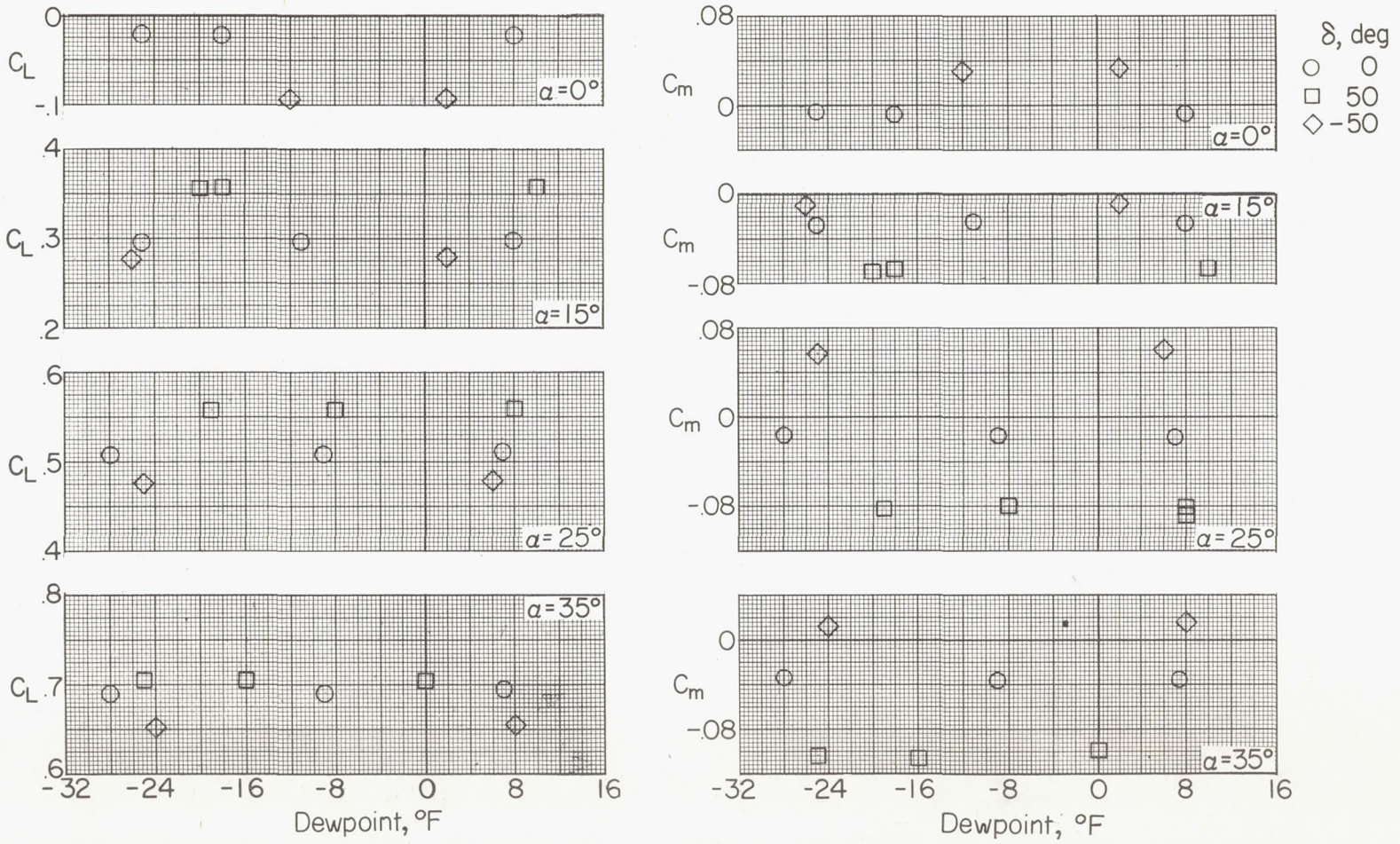

Figure 15.- Effect of variation in dewpoint on the values of C_L and C_m for model A (rectangular holes opened).

CONFIDENTIAL

	Circular disk	Square disk	Triangular disk
Area, sq in.	6.421	6.426	6.458

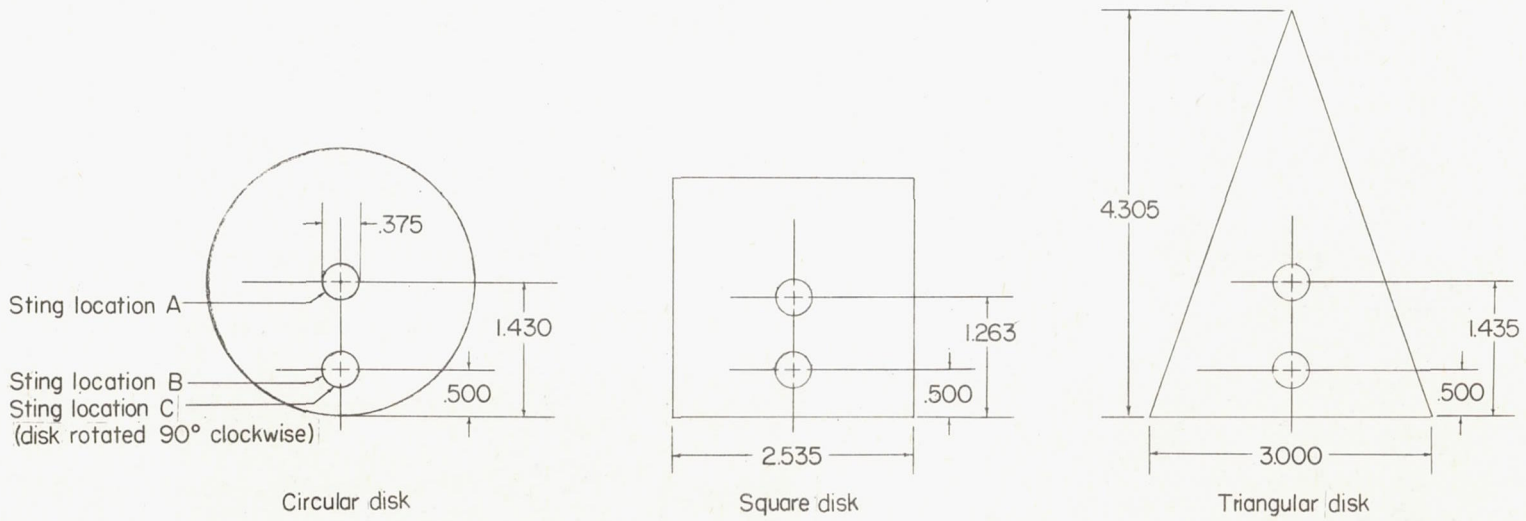

Figure 16.- Drawings of rear view of support-interference disks. All dimensions are in inches.

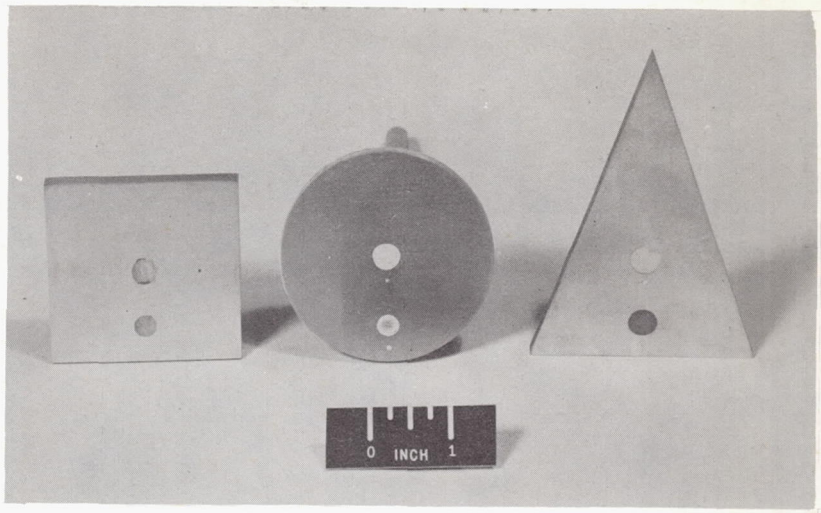

(a) Three disks.

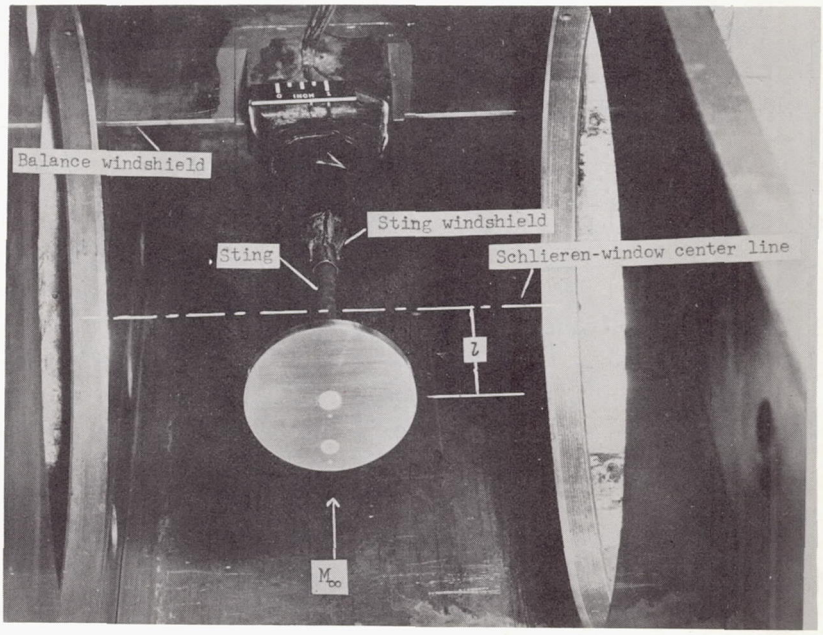

(b) Circular disk mounted in the tunnel. L-60-4281

Figure 17.- Photographs of support-interference disks.

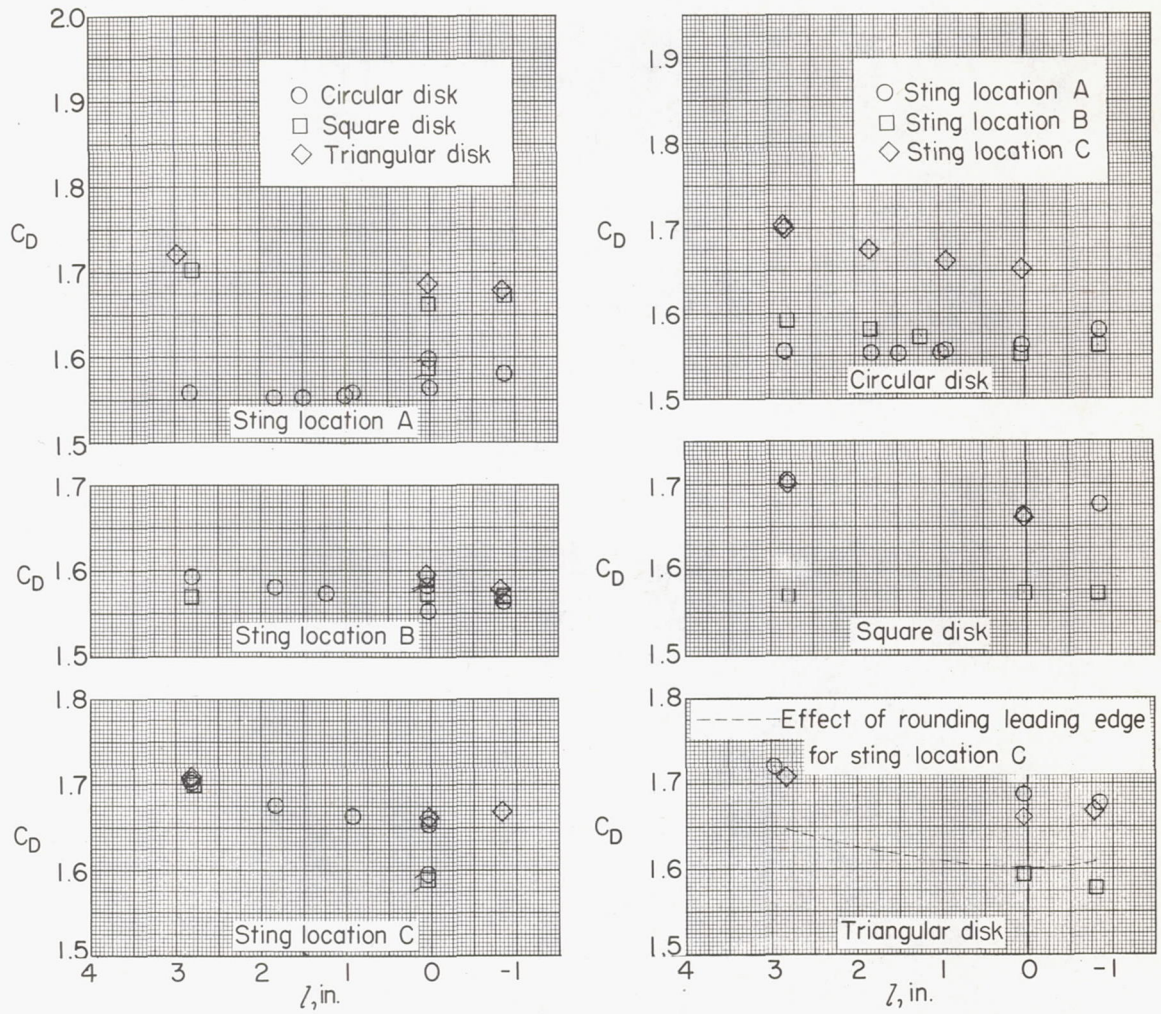

Figure 18.- Variation in value of C_D with sting location, disk shape, and value. (Flagged symbols denote corrected points.)